Hydrogen in Oxides

First Principles and Experimental Studies of Incorporation, Complex Formation, Exotic Species, and Transport Properties

Tor Svendsen Bjørheim

Dissertation for the degree of Philosophiae Doctor

Department of Chemistry
Faculty of Mathematics and Natural Sciences

UNIVERSITY OF OSLO

August 2012

Series of dissertations submitted to the
Faculty of Mathematics and Natural Sciences, University of Oslo
No. 1255

ISSN 1501-7710

Cover: Inger Sandved Anfinsen.
Printed in Norway: AIT Oslo AS.

Produced in co-operation with Akademika publishing.
The thesis is produced by Akademika publishing merely in connection with the thesis defence. Kindly direct all inquiries regarding the thesis to the copyright holder or the unit which grants the doctorate.

Preface

This thesis is submitted in partial fulfillment of the requirements for the degree of Philosophiae Doctor (Ph.D.) at the Department of Chemistry, Faculty of Mathematics and Natural Sciences, University of Oslo, Norway. The work has been carried out at the Department of Chemistry and Functional Energy Related Materials in Oslo (FERMiO) during the period September 2008 to August 2012, under the supervision of Prof. Truls Norby, Assoc. Prof. Reidar Haugsrud and Prof. Svein Stølen.

I would like to thank my three supervisors for their guidance, support and enthusiasm during this period. In retrospect, being supervised by three very different persons with diverse, but complementing scientific background, has been beneficial in my scientific work and personally very motivating. Prof. Svein Stølen deserves special mention; 9 years have now passed since he convinced me to start my Bachelor's degree studies at the University of Oslo during a chemistry lecture at Persbråten high school back in the winter of 2003, for which I am still grateful.

I would also like to thank Dr. Akihide Kuwabara who I got to know while studying for my Master's degree. I was also fortunate enough to work with him for 3 months at the Nanostructures Research Laboratory, JFCC, in Nagoya, Japan in the spring of 2010 during the course of my Ph.D. It was an interesting period of my life which I would never have gone without, and I will forever be thankful for this opportunity.

Further, I would like to express my gratitude to all former and present fellow students and colleagues at the group of Solid State Electrochemistry at the University of Oslo for being excellent colleagues and friends, and making my time in the group interesting and enjoyable. In particular, I would like to thank Anders W. B. Skilbred, Jonathan Polfus, Harald Fjeld, Vasileios Besikiotis, Skjalg Erdal and Camilla Vigen for their fruitful discussions and support.

Finally, I would like to express my deepest gratitude to my friends, and last but not least, to my family, for their endless support and patience.

Oslo, August 2012

Tor Svendsen Bjørheim

Summary

This thesis takes on fundamental studies of various topics related to the behavior of hydrogen defects in functional oxides; aspects related to their thermodynamic stability, possible charge states, complex formation and transport properties. The work encompasses studies of a number of binary and ternary proton and semiconducting oxides and undertakes both first principles Density Functional Theory (DFT) calculations and various experimental techniques.

$PbZrO_3$ is the end-member of the $PbZrO_3$-$PbTiO_3$ (PZT) series of piezoelectric materials, for which hydrogen has been claimed to deteriorate the performance during post-annealing. In this work, the hydration properties of nominally undoped and acceptor doped $PbZrO_3$ are investigated by means of AC conductivity measurements. Further, the enthalpy of hydration of oxygen vacancies for the series $AZrO_3$ (A = Pb, Ca, Sr and Ba) is determined from first principles calculations. $PbZrO_3$ displays mixed p-type electronic and protonic conduction at temperatures below ~700 °C in humid, oxidizing atmospheres, with a defect structure dominated by aliovalent acceptors, Pb vacancies, protons and oxygen vacancies. Experimentally, the hydration enthalpy is determined to -1.07±0.13 eV, while the enthalpy of mobility for protons amounts to 0.93 eV. The hydration enthalpies from first principles calculations are in agreement with those determined experimentally. These results indicate that the hydration enthalpy of perovskite structured oxides to some extent correlate with the absolute value of the difference in electronegativity of the two cations, and also with their Goldschmidt tolerance factor, reflecting that both bonding nature and structure/symmetry affect their hydration enthalpy.

The rare-earth arsenates, $REAsO_4$, are structurally similar to the monazite and scheelite structured $REXO_4$ (X = P, V and Nb), for which significant proton conduction has been reported in literature. In this work, AC conductivity measurements are utilized to investigate the hydration and proton transport properties of nominally undoped and Sr doped $LaAsO_4$. Hydration enthalpies, possible complex formation, and the local atomic structure of protons and oxygen vacancies in $LaAsO_4$ and similar oxides are investigated through first principles DFT calculations. The defect structure of Sr doped $LaAsO_4$ appears to be dominated by oxygen vacancies in the form of pyroarsenate ions, $As_2O_7^{4-}$, in dry atmospheres at high

temperatures, and by protons, or hydrogen arsenate ions $HAsO_4^{2-}$, in wet atmospheres. $LaAsO_4$ is a pure proton conductor below ~850 °C, albeit with lower partial proton conductivity than those of the structurally similar $LaVO_4$ and $LaPO_4$. Nevertheless, the enthalpy of mobility for protons decreases notably with increasing X ion radii in the monazite structured series $LaXO_4$ (X = P, As and V), whereas the hydration enthalpy is less affected by X ion substitution.

Several rare-earth pyrochlore structured oxides, $RE_2X_2O_7$ (X = Ti, Sn, Zr and Ce), have in the recent years been shown to display moderate levels of proton conductivity in wet atmospheres. We investigate trends in the hydration thermodynamics through the pyrochlore series by thermogravimetric (TG) measurements and first principles calculations. From simplified vibrational thermodynamics, we indicate that the hydration entropy can be expected to be similar for similar series of oxides, attributable to only small changes in the bonding environment of oxygen vacancies and protons. Hence, trends in the hydration thermodynamics through the pyrochlore series are dominated by changes in the hydration enthalpy. Both from the TG measurements and DFT, the hydration enthalpy becomes less exothermic with decreasing radii of the RE ion (*i.e.,* from La to Lu). Further, the enthalpy is less affected by X ion substitution, similar to as in the monazite series. The observed trends are finally discussed in relation to the stability, electronic structure and bonding nature of the oxides, and compared with existing trends and correlations for other oxide series.

TiO_2, a wide band gap oxide semiconductor has attracted widespread interest over the last decades, mostly due to its photocatalytic properties and thus utilization in for instance photocatalyzed water cleaning or H_2(g) production. However, the effect of hydrogen defects and Ti vacancies on its defect structure and electrical properties has for long been overlooked. The thesis includes an experimental study of the hydration properties of acceptor doped, bulk, polycrystalline rutile TiO_2, as well as the effect of protons on the n- and p-type conductivity. Furthermore, we investigate the thermodynamic stability of hydrogen related defects, Ti vacancies and their mutual complexes in both bulk and at the (1 1 0) surface of rutile TiO_2 from DFT calculations. Experimentally, acceptor doped rutile TiO_2 is found to be a pure n-type electronic conductor under reducing conditions, and a mixed p-type electronic and protonic conductor under oxidizing conditions up to 800 °C, with an enthalpy of hydration of oxygen vacancies of -1.35±0.17 eV. The hydration enthalpies obtained from DFT calculations are slightly more exothermic (-1.67 to -1.84 eV). From DFT calculations we predict that undoped and donor doped bulk TiO_2 to a large extent is governed by Ti vacancies, protons and their mutual complexes (or Ruetschi type defects) under equilibrium conditions in wet, oxidizing atmospheres, especially at low to moderate temperatures. Further, our results indicate that these defects also will dominate the surfaces of rutile TiO_2 under such conditions. The Schottky formation enthalpy (1.5 eV per defect) of rutile TiO_2 is considerably

more favorable than that of the other binary semiconductors wurtzite ZnO (2.5 eV) and Cr_2O_3 (3.4 eV), and while such defects dominate TiO_2, their equilibrium concentrations in the latter oxides are significantly lower. Interestingly, the stabilization of a cation vacancy by a proton (*i.e.,* binding enthalpy) is most pronounced for the two latter oxides, and we speculate how these observations may be correlated to for instance the bonding nature of the oxides.

Successful realization of ZnO based applications, such as UV light emitting and laser diodes, is subjected to difficulties associated with p-type doping of ZnO, and a persistent n-type conductivity. We investigate the defect structure of ZnO from electrical measurements and first principles calculations to shed light on its persistent n-type conductivity, and the possibility of effective p-type doping of ZnO by Li. Undoped ZnO is dominated by protons, electrons and oxygen vacancies under a large variety of atmospheric conditions, and the equilibrium concentrations of all native acceptor defects are shown to be small. Under the most reducing conditions, we also predict that the more exotic substitutional hydride ion will dominate the defect structure of ZnO, a situation to the best of our knowledge not reported for ZnO before. Based on the results for ZnO, and other binary oxides in this thesis, we argue that this defect could be more important in oxides than previously anticipated, and possibly explain reports of apparent hydride ion transport in solid state ionics research. The equilibrium defect concentrations of hydrogen related and intrinsic defects in ZnO are however small, and are overshadowed by other extrinsic impurities such as Li. Although introduction of Li lowers the Fermi level in ZnO, the material remains n-type, which is attributed both to dominance of various ionic defects and also to passivation of the Li acceptor in the form of the two effectively neutral complexes, $(Li_{Zn}OH_O)^{\times}$ and $(Li_{Zn}Li_i)^{\times}$. We finally propose that one may lower the Fermi level of Li doped ZnO even further under non-equilibrium conditions through rapid quenching from elevated temperatures, which possibly could yield effectively p-type ZnO.

Table of Contents

List of Papers

The thesis includes the following papers:

I. **A combined conductivity and DFT study of protons in $PbZrO_3$ and alkaline earth zirconate perovskites**, T. S. Bjørheim, A. Kuwabara, I. Ahmed, R. Haugsrud, S. Stølen and T. Norby, *Solid State Ionics*, **181**, 2010, 130.

II. **Hydration and proton conductivity in $LaAsO_4$**, T. S. Bjørheim, T. Norby and R. Haugsrud, *Journal of Materials Chemistry*, **22**, 2012, 1652.

III. **Hydration thermodynamics of pyrochlore structured oxides from TG and first principles calculations**, T. S. Bjørheim, V. Besikiotis and R. Haugsrud, *Dalton Transactions*, **41**, 2012, 13343

IV. **Hydration of Rutile TiO_2: Thermodynamics and Effects on n- and p-Type Electronic Conduction**, S. Erdal, C. Kongshaug, T. S. Bjørheim, N. Jalarvo, R. Haugsrud and T. Norby, *Journal of Physical Chemistry C*, **114**, 2010, 9139.

V. **Defect chemistry of rutile TiO_2 from first principles calculations**, T. S. Bjørheim, A. Kuwabara and T. Norby, Submitted, *Journal of Physical Chemistry C*, 2012.

VI. **Defects at the (1 1 0) surface of rutile TiO_2 from ab initio calculations**, T. S. Bjørheim, A. Kuwabara, C. E. Mohn and T. Norby, *International Journal of Hydrogen Energy*, **37**, 2012, 8110.

VII. **H and Li related defects in ZnO and their effect on electrical properties**, T. S. Bjørheim, S. Erdal, K. M. Johansen, K. E. Knutsen and T. Norby, *Journal of Physical Chemistry C*, 2012, 10.1021/jp307835c

In addition, I have contributed to the following publications:

VIII. **Ab initio studies of hydrogen and acceptor defects in rutile TiO_2**, T. S. Bjørheim, S. Stølen and T. Norby, *Physical Chemistry, Chemical Physics*, 12(25), 2010, 6817

IX. **The role of B-site cations on proton conductivity in double perovskite oxides La_2MgTiO_6 and La_2MgZrO_6**, C. K. Vigen, T. S. Bjørheim, R. Haugsrud, *International journal of hydrogen energy*, **37**(9), 2012, 7983

X. **Nitrogen defects in wide band gap oxides: Defect equilibria and electronic structure from first principles calculations**, J. M. Polfus, T. S. Bjørheim and R. Haugsrud, *Physical Chemistry, Chemical Physics,* **14**, 2012, 11808

1. Introduction

Mankind has since ancient times benefitted from utilization of materials in everyday life, where the materials of choice in a period of time have named the era. This is also true in our modern world, where the desire for continuous technological advancements drives the development of smarter and increasingly more advanced materials with specific *functional* properties. This development has led to the research field known as *materials science*. In materials science, concepts from all the natural sciences are combined to develop and relate the functional properties of materials to their atomic composition and structure. Materials science has in the past decades moved from traditionally being an experimental research field to also witness a tremendous increase in the utilization of various computational techniques.

The techniques of computational materials science are at any point limited by the available computational resources. Computational studies were therefore until the last decade limited to 'classical', potential based simulations. Despite their simplicity, such techniques in many cases offer valuable insight into materials properties and phenomena [1-5]. Nowadays, most researchers however prefer so-called *ab-initio* techniques which are derived from first principles, and are thus in theory exact. Today's workhorse in computational materials science is *Density Functional Theory* (DFT) [6-9], which is also utilized throughout this thesis. Whereas an experimental study often is both time and cost-consuming and may involve hazardous materials, a computational DFT study simply requires a decent supercomputer, the atomic structure of the material to be simulated, in addition to the DFT code which describes the interactions between all electrons and ions in a suitable manner. The reader should however note that such studies are by no means trivial and require careful choice of approximations and algorithms, and often extensive test calculations. Although such techniques, being ground state techniques, inherently omit temperature effects, materials properties obtained from DFT may be extrapolated to finite temperature through combination with thermodynamic modeling.

Hydrogen is the lightest and most abundant chemical element in the universe. In our daily life, it is omnipresent either as water vapor or hydrogen gas and is found to constitute a major *defect* in the form of *protons* in many functional materials. A wide range of oxides absorb protons at temperatures exceeding 1000 °C and even display significant levels of *protonic*

conduction. Such oxides find both potential and realized utilization in gas separation membranes, catalytic membrane reactors, photocatalytic applications, proton conducting fuel cells and gas sensors. Protons, being small and highly mobile in oxides, may interact and bond to a variety of other defects in the form of *complexes*. Although association complexes in many cases are overlooked, they may to a large extent dominate the defect structure of for instance acceptor doped oxides, and thus greatly affect their functional properties [10]. In other oxides, unintentional introduction of hydrogen defects is highly undesirable. For instance in semiconductor based devices, whose functional properties rely on careful control of all impurities, hydrogen defects may act as a source of doping, and thus to a large extent dominate the materials' electrical properties [11]. The behavior of hydrogen in oxides is however not limited to the 'simple' protonic defect, and hydrogen may in principle take on either of its three charge states, +1, 0 or -1, in oxides [12]. In that respect, several authors have in the last decade speculated about the possible presence of hydride ion related defects in oxides and whether such defects may dominate the electrical properties under the most reducing conditions [13-17]. The behavior of hydrogen in oxides is thus diverse, and not always trivial to predict. As such, whether working with materials where protons are desirable or not, a fundamental knowledge of the behavior of hydrogen related defects; their thermodynamic stability, possible exotic species, association with other point defects, and transport properties, is essential for both the understanding and utilization of such materials.

1.1 Thesis outline

The thesis is based on 7 papers, covering various binary and ternary oxides; $PbZrO_3$ and similar perovskite structured oxides (Paper 1), $LaAsO_4$ and similar monazite oxides (Paper 2) pyrochlore oxides (Paper 3), rutile TiO_2 (Paper 4-6) and wurtzite structured ZnO (Paper 7). These materials are of interest due to different functional properties; while the materials in Paper 1-3 mainly are studied for their protonic transport properties, TiO_2 and ZnO in Paper 4-7 are of interest due to their semiconducting properties. Nevertheless, the behavior of hydrogen is a common denominator throughout the papers; compositional and structural trends in its thermodynamic stability, exotic hydrogen species and interactions with effectively negatively charged acceptor defects. The thesis includes both experimental and computational considerations, and a major focus point is to further emphasize the strengths of first principles techniques in materials science.

$PbZrO_3$ is an antiferroelectric and the end-member of the piezoelectric series $PbZrO_3$-$PbTiO_3$ (PZT), for which hydrogen has been claimed to deteriorate the performance during *post*-annealing. Although Pb based oxides are unsuitable for proton conduction applications due to the volatile nature of PbO, determination of the hydration properties of $PbZrO_3$ is of interest to predict trends in the hydration properties of perovskite structured oxides in general. Paper 1 investigates the transport and hydration properties of Pb deficient and Y doped $PbZrO_3$, and

the alkaline-earth zirconate perovskite oxides, $AZrO_3$ (A = Ca, Sr and Ba), through conductivity measurements and first principles defect calculations.

Significant proton conduction has been reported in wet atmospheres for a variety of monazite and scheelite structured oxides, $REXO_4$ (RE = La-Lu, X = P, As, V and Nb), for which the highest are found among those of the rare-earth ortho-phosphates, $REPO_4$, and ortho-niobates, $RENbO_4$. A natural continuation along this series of oxides is therefore the rare-earth ortho-arsenates, $REAsO_4$. Although As containing compounds are considered hazardous, determination of the effect of substituting P with the larger As on the proton transport properties provides insight into the compositional dependence of the proton transport properties of such oxides. In Paper 2 we study the transport and hydration properties of acceptor doped $LaAsO_4$ using AC conductivity measurements, and elaborate on the nature of oxygen vacancies and protons in $LaAsO_4$ and similar oxides using first principles calculations.

Rare-earth pyrochlore structured oxides, $RE_2X_2O_7$ (X = Ti, Sn, Zr and Ce), are interesting candidates as proton conductors at intermediate temperatures, albeit with somewhat lower maximum proton conductivities than the perovskites. For perovskites, trends in hydration thermodynamics and proton transport properties are attributed changes in the structure/symmetry and the difference in electronegativity of the two cations (or basicity) through the series. Pyrochlore oxides however retain a cubic structure for a large variety of compositions, and only display minor electronegativity changes through the series. Trends and changes in the hydration thermodynamics through the series may thus possibly be related to the elemental composition of the oxides alone. In Paper 3 we investigate trends in the hydration properties through the pyrochlore series using thermogravimetric measurements and first principles calculations, and discuss the observed trends in connection with correlations for other series of proton conducting oxides.

TiO_2, a wide band gap oxide semiconductor, has since the discovery of its photocatalytic properties in the 1970s, attracted widespread attention. It finds usage in numerous potential and realized applications, for instance photocatalyzed water cleaning or H_2(g) production. Although such and similar applications involve exposure of TiO_2 to either humid atmospheres or liquid H_2O, the effect of protonic defects on its defect structure and electrical properties has been neglected until very recently. In addition, it has been speculated whether Ti vacancies, and hydration of these, could play an important role in TiO_2. In Paper 4-6 we determine the hydration thermodynamics of rutile TiO_2 experimentally and computationally, and investigate the possible dominance of Ti vacancies and hydration of these at lower temperatures in bulk and at surfaces of rutile TiO_2 using first principles defect calculations and thermodynamic modeling.

Another oxide semiconductor which has become increasingly popular in the recent years is ZnO. It finds potential applications in for instance UV light emitting diodes (LED) and laser diodes. However, the successful realization of such applications is hindered by the lack of stable and reproducible p-type doping of ZnO. Although there are claims that for instance Li doping has resulted in effectively p-type ZnO, there are few papers supporting these reports. The last paper presented in this thesis is dedicated to elaborating on the dominant n-type activity of ZnO, and the possibility of stable p-type doping by Li, with emphasis on the effect of hydrogen defects. The work undertakes both electrical measurements on Li doped single crystalline ZnO, and first principles calculations.

Before presenting the papers, I will introduce the reader to the basic concepts of the first principles technique utilized in this thesis, DFT. Further, I will show how such calculations may be used to predict finite temperature defect structures through thermodynamic modeling, before covering some common mistakes and pitfalls when employing such calculations. The thesis will be summarized by a general discussion of various topics encountered in the presented papers.

2. Theoretical approaches

Over the last decades, there has been a tremendous progress in the development and utilization of first principles calculations in simulation of materials properties and processes[8]. The workhorse of this development is density-functional theory (DFT) which transforms the intricate complexity of the electron-electron interactions encountered in many-particle systems to a more manageable system described simply by the electron density. As the audience of this thesis is materials scientists, the intent of the following chapter is to give the reader a brief overview of the basic concepts of DFT, its most common implementations, approximations, encountered pitfalls and shortcomings. Further, I will focus on how such calculations may be utilized in combination with thermodynamic modeling and concepts from the field of defect chemistry to predict finite temperature defect concentrations and defect-dependent properties.

2.1 Density Functional Theory

The need for approximations when solving many-particle problems stems from the complexity of systems with a larger number of mutually interacting electrons. The Born-Oppenheimer approximation simplifies the problem somewhat by assuming stationary nuclei, yielding the simplified Hamiltonian for the electronic system:

$$\hat{\mathrm{H}}_{\mathrm{e}} = T_{\mathrm{e}}[\boldsymbol{r}] + V_{\mathrm{e-e}}[\boldsymbol{r}] + V_{\mathrm{e-n}}[\boldsymbol{r}, \boldsymbol{R}] \tag{1}$$

where $T_{\mathrm{e}}[\boldsymbol{r}]$ represents the electrons' kinetic energy, $V_{\mathrm{e-e}}[\boldsymbol{r}]$ the electron-electron interactions, and $V_{\mathrm{e-n}}[\boldsymbol{r}, \boldsymbol{R}]$ the electron-core interactions. However, the complexity of the problem still increases rapidly with the size of the system.

The basis for DFT was formulated in 1964 by Hohenberg and Kohn [6], who stated that, for an electronic system of interacting particles in an external potential $V_{\mathrm{ext}}(\mathbf{r})$, the potential is, to within a constant, uniquely determined by the ground state electron density, $n_0(\mathbf{r})$. Hence, all properties of the system are also determined by $n_0(\mathbf{r})$. Secondly, they stated that there exists a universal energy functional for which the global minimum yields the ground state energy:

$$E[n(\mathbf{r})] = T[n(\mathbf{r})] + J[n(\mathbf{r})] + E_{\mathrm{ncl}}[n(\mathbf{r})] + \int n(\mathbf{r}) V_{\mathrm{ext}}(\mathbf{r})\, \mathrm{d}\mathbf{r} \tag{2}$$

where $T[n(\mathbf{r})]$ is the kinetic energy, $J[n(\mathbf{r})]$ the Coulombic electron-electron interactions, $E_{\mathrm{ncl}}[n(\mathbf{r})]$ encompasses non-classical electron-electron interactions due to exchange and correlation, and the last term represents the interactions between electrons and the core potential. While the Hohenberg-Kohn formalism applies to a system of interacting particles, Kohn and Sham[7] devised a practical scheme for solving the universal functional by mapping the system of interacting electrons onto a non-interacting reference system built from a set of orbitals (or one-electron functions). This approach allows determination of a larger part of the system's kinetic energy (*i.e.,* kinetic energy of the non-interacting electrons, $T_{\mathrm{ni}}[n(\mathbf{r})]$), while the remainder is merged with the 'unknown' non-classical electron-electron interactions in the so-called exchange-correlation functional, $E_{\mathrm{XC}}[n(\mathbf{r})]$:

$$E[n(\mathbf{r})] = T_{\mathrm{ni}}[n(\mathbf{r})] + J[n(\mathbf{r})] + E_{\mathrm{XC}}[n(\mathbf{r})] + \int n(\mathbf{r}) V_{\mathrm{ext}}(\mathbf{r})\, \mathrm{d}\mathbf{r} \qquad (3)$$

The Kohn-Sham formalism is thus in principle exact (hence the term *ab initio* or first principles). However, the approximations needed to determine $E_{\mathrm{XC}}[n(\mathbf{r})]$ renders all DFT codes inexact and development of modern DFT is to a large extent focused on development of more accurate and correct XC functionals.

2.2 XC functionals

While the most popular XC functionals within molecular chemistry usually are semi-empirical functionals parameterized to a given set of experimental data, solid state physicists and chemists rely on functionals with less degree of empiricism. The latter class of functionals can loosely be ranged according to their 'level of theory'; (i) the local density approximation (LDA), (ii) generalized gradient approximation (GGA), (iii) LDA/GGA with corrections for on-site Coulomb repulsion (+U) and (iv) hybrid functionals.

LDA[7], the simplest approximation to the XC contributions, approximates the XC energy at each point to that in a homogenous electron gas of density $n(\mathbf{r})$. While the exchange part in a homogeneous electron gas is exact, the correlation part is obtained by Quantum Monte Carlo simulations. There are many LDA parameterizations, with the most recent being that of Perdew and Zunger [18]. Despite its simplicity, LDA works surprisingly well for systems without large local variations in the electron density, but overestimates bond strengths somewhat, underestimates lattice constants and gives erroneous metallic ground states [9].

The electron density in real systems is however rarely constant, not even on a local scale. The natural improvement is thus introduction of the XC functional's dependence on gradients in the electron density, as in the GGA based functionals. In GGA, the XC energy is thus a functional of both the electron density itself, and its gradient $\nabla n(\mathbf{r})$. There exists an extensive selection of GGA functionals, differentiated by how the dependence of the exchange and correlation energy on $\nabla n(\mathbf{r})$ is described, and the functionals are usually named after their

developers. The most commonly adopted GGA functionals today are those proposed by Perdew and Wang [19] (PW91) and by Perdew, Burke and Ernzerhof (PBE) [20]. While the PW91 functional is constructed using quantum monte carlo simulations for the electron gas, PBE is constructed using exact properties of the XC energy[9, 20]. In general, GGA to some extent corrects the overbinding tendency of LDA functional, however, with an opposite tendency to underbind somewhat [9]. As such, while LDA underestimates lattice constants by 1% on average, GGA overestimates them by nearly the same amount, resulting also in errors in other parameters that are sensitive to volume/bonding lengths such as phonon frequencies and bulk modulus. Both LDA and GGA functionals heavily underestimate band gaps of semiconductors, especially in strongly correlated materials such as d- and f-electron systems (*cf.* ref. [9] and references therein).

GGA and LDA based functionals are unable to account for the strong Coulomb repulsion between electrons occupying for instance narrow 3d bands and localized orbitals. DFT+U techniques attempt to correct this by adding a Hubbard-type Coulomb repulsion in the form of a *U* term to the DFT Hamiltonian. The +U technique improves band gaps, magnetic ordering and reproduces localized solutions in 3d systems. The *U* term is an adjustable parameter, often fitted to for instance spectroscopic results and DFT+U techniques are thus semi-empirical. However, the empiricism of the approach may lead to unphysical results due for instance to too large, or compositional dependent (in for instance defect calculations) Coulomb on-site repulsions.

Hybrid functionals are functionals that combine the strengths of DFT and Hartree-Fock (HF) theory in description of the XC energy. This development is rationalized by that DFT often yields too small band gaps while HF yields too large band gaps. Further, the exchange part of the electron-electron interactions is exact within HF, while the formalism does not encompass the correlation part. Hence, hybrid functionals are constructed by intermixing a given percentage exact HF exchange with the DFT exchange, while the correlation part is treated by means of the DFT XC functional:

$$E_{\mathrm{XC}}^{\mathrm{Hybrid}} = (1-a)E_{\mathrm{X}}^{\mathrm{DFT}} + aE_{\mathrm{X}}^{\mathrm{HF}} + E_{\mathrm{C}}^{\mathrm{DFT}} \quad (4)$$

The most popular hybrid functionals in solid state materials science are PBE0 [20] and HSE03 (and HSE06) [21, 22]. Determination of the long range HF exchange is computationally demanding, as in the unscreened PBE0 functional. In that respect, Heyd, Susceria and Ernzerhof (HSE) [21, 22] proposed to apply the HF exchange only to short range interactions, while treating the long range interactions only with DFT, and the HSE based functionals are thus somewhat less computationally demanding than PBE0. In all functionals, the default setting is 25% HF exchange and all may in principle be used in combination with either LDA or GGA functionals (although GGA-HSE is most common). However, especially in defect

calculations that rely on accurately determined band gaps, it is common to adjust the HF intermixing fraction so as to match the theoretical band gap of the system of interest with the experimental one. As recent examples, Oba *et al.* [23] used 37.5% HF exchange for ZnO while Janotti *et al.* [24] used 20% for rutile TiO_2.

2.3 Practical implementation: Plane waves, k-points and potentials

Practical implementations of DFT for solving electronic structure problems fall in two broad classes; plane-wave methods and those utilizing localized basis functions. The former type, such as for instance the Vienna *Ab-initio* Simulation Package (VASP) [25-28], has gained most attention within materials science and in studies of periodic crystalline systems. Localized basis sets require a large number of basis functions for convergence. Control of the convergence of a plane-wave basis is on the other hand trivial, as it in principle is sufficient to monitor for instance the total energy convergence as a function of the *cut-off energy*, *i.e.* the highest kinetic energy used for expansion of the plane-wave basis. The higher the cut-off energy, the more complete is the basis set, and the more computationally demanding are the calculations.

Further simplification of the electronic structure problem is commonly achieved by exploiting the fact that wave functions at **k**-points (*i.e.,* reciprocal lattice vectors within the first Brillouin zone) close to each other are similar. Hence, instead of calculating the wave functions at an infinite number of **k**-points, it suffices to evaluate them at a finite, selected number of **k**-points using an appropriate extrapolation scheme for the remainder of the Brillouin zone. The number of required **k**-points depends on the size of the system, and is usually reported as the number of **k**-points in each orthogonal direction, or the **k**-point density.

Although there exist several all-electron plane-wave codes (for instance Wien2k [29]), the *pseudopotential* approach avoids treatment of the strongly bound and chemically inert core electrons by replacing them with a constant potential and only the outermost valence electrons are treated self-consistently. Neglecting the core electrons may however result in an incorrect shape of the wave functions of the valence electrons compared to all electron calculations. The projector augmented wave (PAW) method [30], which is used in this thesis, attempts to combine the efficiency of pseudopotential calculations with the accuracy of all electron calculations, by reconstruction of the all electron wave functions from the pseudopotentials.

The periodic boundary conditions of plane-wave codes allow studies of infinite periodic systems. Aperiodic systems, such as a defective crystal, thus require a larger *supercell* in order to avoid spurious interactions between the defect and its neighboring images. The required supercell size in defect calculations is system dependent, and typical supercells contain up to 750 atoms in LDA/GGA calculations and up to ~150 in hybrid calculations (due to the larger computational costs associated with hybrid functionals calculations). Similarly,

in surface calculations the common approach is application of a slab model (see Figure 1). The slab is periodic (or infinite) in two directions, and aperiodic in the third, where the periodically repeating slabs are separated by a vacuum level. The slab itself should be thick enough to reflect both bulk properties in its center, and surface properties, while the vacuum layer should be thick enough to avoid interactions between the periodic slabs. The common strategy is thus to increase the slab and vacuum layer thickness until the electronic structure (for instance band gap) at the center of the slab reflects bulk and the surface energy converges. The slab model thus includes *two* surfaces, and the terminations should be chosen so that the two surfaces are identical. In surface defect studies, the defect should thus be introduced at each side of the slab to conserve its symmetry and avoid spurious relaxation effects and surface dipoles.

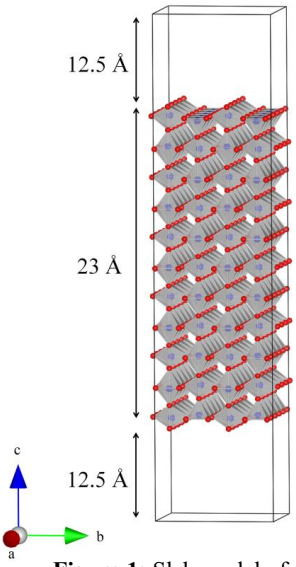

Figure 1: Slab model of the (1 1 0) rutile surface

In practical DFT calculations, the user supplies the potential for each element in the system, exchange correlation functional, 'trial' structure of the system, convergence criteria, optimization algorithms/routines and **k**-point mesh. VASP includes various routines for optimizing the electronic system self-consistently, which is relaxed to the Born-Oppenheimer surface in each atomic step, yielding (among other parameters) the systems *total electronic energy* (referred to as E^{tot}). The atomic system may similarly be optimized by minimization of the forces acting on all atoms after reaching electronic convergence until for instance the residual forces are lower than some desired convergence criterion. Hence, upon full structural optimization, the system is in principle relaxed to its ground state structure. However, to ensure physical solutions, small atomic displacements are usually chosen in the relaxation routines and structures separated by larger energy barriers are thus unreachable through structural optimizations alone. For instance, starting from the cubic high temperature structure of the perovskite $SrZrO_3$ will not yield the true ground state orthorhombic perovskite structure. This thus allows studies of non-ground state structures or local minima separated from the true global minima by sufficient energy barriers. As will be pointed out in the final section of this chapter, calculations of non-ground state structures are sometimes non-trivial, especially when the local minima are separated from the global minima by a small barrier.

2.4 DFT and defect thermodynamics

Defect formation

The major part of this thesis deals with the properties of dilute defects in solid (oxidic) matrices. The thermodynamic stability of a defect is governed by its formation energy, $\Delta G^{\mathrm{f}}_{\mathrm{defect}}$, which may be split in four distinct contributions (*cf.* Oba *et al.*[31]):

$$\Delta G^{\mathrm{f}}_{\mathrm{defect}} = \Delta G^{\mathrm{f,electronic}}_{\mathrm{defect}} + \Delta G^{\mathrm{f,vibr.solid}}_{\mathrm{defect}} + \Delta G^{\mathrm{f,vibr.atomic}}_{\mathrm{defect}} + p\Delta V^{\mathrm{f}} \qquad (5)$$

$\Delta G^{\mathrm{f,electronic}}_{\mathrm{defect}}$ is the change in the total electronic energy (as emerging for instance from VASP), $\Delta G^{\mathrm{f,vibr.solid}}_{\mathrm{defect}}$ represents vibrational contributions from within the crystal itself, $\Delta G^{\mathrm{f,vibr.atomic}}_{\mathrm{defect}}$ are vibrational contributions due to exchange of atomic species with the surrounding atmosphere, while $p\Delta V^{\mathrm{f}}$ stems from volume expansion of the crystal upon defect formation. The volume expansion is usually negligible for small defect concentration, and the *p*-*V* term will thus not be considered further.

When neglecting temperature effects, the formation energy may be evaluated according to:

$$\Delta G^{\mathrm{f}}_{\mathrm{defect}} = E^{\mathrm{tot}}_{\mathrm{defect}} - E^{\mathrm{tot}}_{\mathrm{bulk}} + \sum_1^i \Delta n_i \mu_i \; + q(\varepsilon_{\mathrm{f}} + \Delta\epsilon) \qquad (6)$$

where $E^{\mathrm{tot}}_{\mathrm{defect}}$ and $E^{\mathrm{tot}}_{\mathrm{bulk}}$ are the total energies of the defective and pristine supercells, respectively, Δn_i is the change in number of atomic species *i* with chemical potential μ_i upon defect formation. q is the effective formal charge of the defect, ε_{f} the chemical potential of electrons (μ_{e}), or the Fermi level, while $\Delta\epsilon$ aligns the core potentials of the defective and pristine supercells[32]. In the ground state limit, the formation energies are evaluated using a suitable set of atomic chemical potentials, for instance the total energies of the pure phases, for instance $\mu^{\circ}_{\mathrm{H}} = \frac{1}{2}E^{\mathrm{tot}}_{\mathrm{H_2}}$, $\mu^{\circ}_{\mathrm{H_2O}} = E^{\mathrm{tot}}_{\mathrm{H_2O}}$ and $\mu_{\mathrm{O}} = \mu^{\circ}_{\mathrm{H_2O}} - 2\mu^{\circ}_{\mathrm{H}}$.

The simplest approach to extrapolate 0 K defect formation energies to finite temperatures is to assume that $\Delta G^{\mathrm{f,vibr.solid}}_{\mathrm{defect}}$ in Eq. 5 is small, and that atomic species dominate the entropy change upon defect formation. This is achieved by including the temperature and partial pressure dependency of the chemical potentials of all involved atomic species through:

$$\mu_{\mathrm{i}}(T,P) = \mu^{\circ}_{\mathrm{i}} + H_{\mathrm{i}}(T,p^{\circ}) - TS_{\mathrm{i}}(T,p^{\circ}) + k_{\mathrm{b}}T\ln(\tfrac{p_{\mathrm{i}}}{p^{\circ}}) \qquad (7)$$

where μ°_{i} is set to the total energy of the pure phases as obtained from first principles calculations while the second and third terms usually are taken as tabulated temperature dependencies. Although neglecting all solid state vibrational contributions, the use of this approach has been justified in for instance ref. [33], and is adopted throughout this thesis.

The final term in Eq. 5, $\Delta G_{\text{defect}}^{\text{f,vibr.solid}}$, may be evaluated from the change in all vibrational modes within the crystal upon defect formation. This thus requires extensive phonon calculations, including collective vibrations, for accurate evaluation. The problem may be simplified by assuming that all modes in the crystal are independent and purely harmonic, *i.e.* each ion vibrates as a harmonic oscillator for which the free energy is given by:

$$G_i(T) = \frac{\mathrm{h}\nu_i}{2} + k_{\mathrm{b}}T\ln[1 - \exp(-\frac{\mathrm{h}\nu_i}{k_{\mathrm{b}}T})] \quad (8)$$

where ν_i is the frequency of the lattice mode. In this work, I will touch upon the effects of this approach in Paper 3 and in the discussion part of the thesis.

Defect formation energies are in the literature usually only presented as a function of the Fermi level in the 0 K limit, as is illustrated for ZnO in Figure 2. If interpreted correctly, such figures offer detailed information regarding the defect structure:

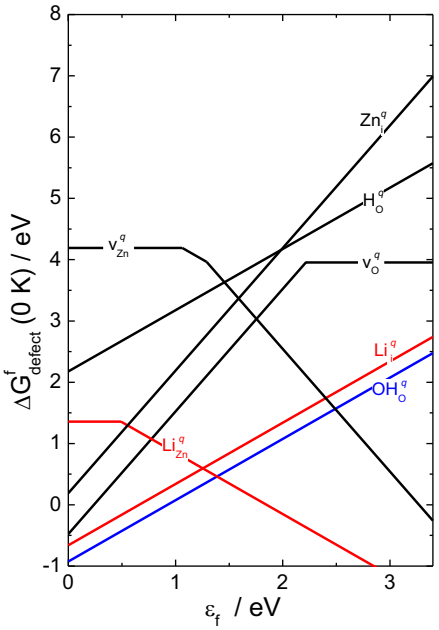

Figure 2: Defect formation energies in ZnO as a function of the Fermi level within the theoretical band gap from Paper 7

- The slopes of the lines reflect the defects' charge state at a given Fermi level.
- The transition points reflect the Fermi level at which a defect changes charge state (thermodynamic transition level). If these levels fall >3k_{b}T from either band edge, the defect is termed deep, while defects with transition levels at or within the valence and conduction bands are termed shallow. The majority of for instance $v_{Zn}^{\times}$ will only be

ionized when the Fermi level is >1.3 eV, or at high temperatures where the thermal energy is in the range of 1.3 eV.

- The lower the formation energy of the defect, the more likely it is to dominate.
- The lowest (formation energy-wise) crossing point between positive and negative defects represents the charge neutrality level. These defects will dominate concentration-wise, determine the electroneutrality and pin the Fermi level.

Equilibrium thermodynamics of point defect formation

Although results such as those in Figure 2 are important, a material's finite temperature, equilibrium defect structure is ultimately connected to the chemical potential of all possible point defects. From the configurational entropy associated with distribution of N_{defect} defects on N regular positions/lattice sites, and hence N-N_{defect} regular particles, it may be shown that the chemical potential of a defect equals [34]:

$$\mu_{\text{defect}} = \mu^{\circ}_{\text{defect}} + RT\ln\left(\frac{N_{\text{defect}}}{N-N_{\text{defect}}}\right) \tag{9}$$

which at $\mu_{\text{defect}} = 0$ yields:

$$\frac{N_{\text{defect}}}{N-N_{\text{defect}}} = \exp\left(-\frac{\mu^{\circ}_{\text{defect}}}{RT}\right) = \exp\left(-\frac{\Delta G^{\text{f}}_{\text{defect}}}{RT}\right) \tag{10}$$

The fraction on the left side of Eq. 10 now expresses the ratio of defects to that of regular particles on a given lattice site, and may be substituted with the species' concentrations (c_i or [species i]). The right side of Eq. 10 contains the free energy of formation (according to Eq. 5) to be expended locally. Since more than one defect may occupy a given regular lattice site, it is convenient to replace the concentration of regular particles at site s by the general symbol $c_{s,0}$, and that of the lattice site by c_s. As such, the general form of Eq. 10 may be written:

$$\frac{c_{\text{defect}}}{c_{s,0}} = \exp\left(-\frac{\Delta G^{\text{f}}_{\text{defect}}}{RT}\right) \tag{11}$$

and the concentration of all $j\epsilon[1,m]$ defects and regular particles at the regular lattice site s must fulfill:

$$\sum_{j=1}^{m} c_j + c_{s,0} = c_s \tag{12}$$

Further, a defective macroscopic crystal must remain effectively neutral. The equilibrium Fermi level will therefore be determined by the concentration of all point defects. More precisely, the Fermi level is pinned so that the concentration of all $i\epsilon[1,M]$ effectively charged species of charge q_i satisfies:

$$\sum_{i=1}^{M} q_i c_i + p - n = 0 \tag{13}$$

Here, c_i, and p and n are for instance volume concentrations. Solving Eqs. 11-13 at each atmospheric condition and temperature for all defects j and charged species i at all involved sites s thus yields the equilibrium defect concentrations in the material. Although in principle simple, this approach is rarely adopted in literature, possibly due to the large computational cost associated with calculation of *all* possible defects in a material.

2.5 Sources of errors and common pitfalls

While errors due to for instance poor convergence of the basis sets and **k**-meshes are easily controlled, finite size errors and errors inherent within the applied XC functionals require more careful control.

XC functionals, localization and band gaps

It is well known that 'classical' XC functionals such as LDA and PBE suffer from underestimation of band gaps, which in itself poses a significant error in the chemical potential of electrons and thus the formation energies of charged defects. Further, especially localized 3d states are poorly described and both functionals tend to delocalize such states. Although the two problems are interlinked, their effects on defect properties are different. Oxygen vacancies in ZnO and TiO_2 are good examples; removal of an O in the two oxides results in 4 and 3 dangling Zn and Ti bonds, respectively. In ZnO, these 4 states result in a fully symmetric defect state, which may accommodate up to two electrons and the vacancy itself may thus exist in three possible charge states $v_O^{\times}$, $v_O^{\bullet}$ and $v_O^{\bullet\bullet}$ [35]. For ZnO, LDA and PBE are able to describe this localized state, but the severe underestimation of the band gap (0.7 eV in LDA *vs.* 3.4 eV experimentally [35]) renders determination of the thermodynamic transition levels highly uncertain (see Figure 3). Although various extrapolation schemes using LDA and LDA+U determined formation energies exist [35], hybrid functionals, which

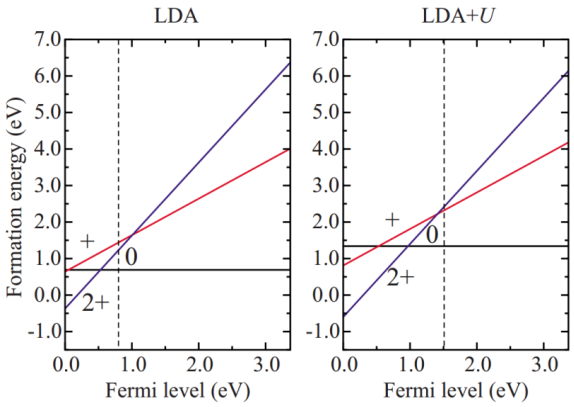

Figure 3: Formation energies of oxygen vacancy in its three possible charge states in ZnO with LDA and LDA+U from Janotti and van de Walle [35].

yield more accurate band gaps, are now routinely applied to determine such transition levels [23].

The nature of the oxygen vacancy related defect state in TiO_2 is slightly different from that in ZnO; while the state is symmetrical and centered at the vacancy itself in ZnO, the electrons occupying the state in TiO_2 are centered at Ti ions neighboring the vacancy. In LDA/PBE structural relaxation pushes this state above the conduction band, and completely delocalize the solution for $v_O^{\times}$ and $v_O^{\bullet}$, thus rendering determination of their transition levels impossible (see Paper 5 and Janotti *et al.* [24]). PBE+U and hybrid functionals on the other hand yield the correct ground state with either 1 or 2 electrons localized on the neighboring Ti ions (see Paper 5).

However, one should note that not even hybrid functionals are perfect, as it is customary to adjust the fraction of HF exchange to match the experimental band gap. In that respect, Lany and Zunger [36] recently argued, based on single-shot quasi-particle GW calculations, that in doing so for ZnO, the (+2/0) transition level of oxygen vacancies is pushed too close to the conduction band. However, this topic is still debated, and future completely self-consistent GW-HSE calculations are required to elucidate the effects of this approximation.

Underestimation of the band gap also has a second effect; the formation energies of defects are calculated with respect to the band edges of the oxide (for instance the top of the valence band), and over/underestimation of the position of the band edges thus yields a significant error in the formation energies. This is illustrated in Figure 4 from Paper 5 showing the 0 K formation energies of various point defects in rutile TiO_2 calculated with PBE and the HSE functional. The band gap opens from 1.77 (PBE) to 3.01 eV (HSE), which Janotti *et al.* [24] showed to be due to a downward shift of the valence band (VB) edge by 0.6 eV and an upward shift of the conduction band (CB) by 0.7 eV.

The formation energy of the neutral oxygen interstitial, $O_i^{\times}$, is unaffected by changes in the band edges and PBE and HSE thus give comparable formation energies. However, the formation energies of all the charged defects at for instance $\mu_e = 0$ eV differ significantly. However the PBE formation energies at $\mu_e = 0.0$ eV are closer to the HSE values evaluated at $\mu_e = 0.6$ eV (*i.e.*, at the energy of the VB edge in PBE). Similarly, the Fermi level in Figure 4 would be pinned approximately where $\Delta G^{f}_{OH_O^{\bullet}} = \Delta G^{f}_{v_{Ti}^{4/}}$ which falls at 0.9 and 1.6 eV above VB at formation energies of 0.11 and 0.17 eV in PBE and HSE, respectively. This again means that the two functionals would predict similar equilibrium defect concentrations of the ionic

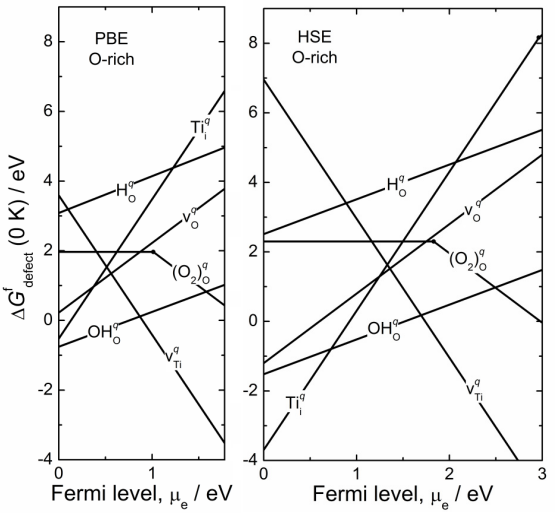

Figure 4: Defect formation energies in rutile TiO_2 at 0 K using PBE and HSE from Paper 5.

defects. However, while PBE yields a Fermi level pinned in the p-type region and thus predicts p > n, HSE yields a n-type material. The choice of functional thus mainly affects the concentration of electronic defects under thermal equilibrium, in addition to the defects' transition levels.

Molecules and chemical potentials

As mentioned in the preceding section, LDA and GGA-PBE have a tendency to over- and underbind systems, respectively. The average error in calculated lattice parameters is ~1% [9], and has small effects on the total energy of solids. Hence, total energy differences involving only defect free solids, such as the formation energy of ternary oxides, are well reproduced (*cf.* Martinez *et al.* [37]).

Poor treatment of small molecules in LDA/PBE and plane-wave codes is however a more severe problem. The O_2 molecule is for instance overbound by 1.0 eV [38], which results in an error of 0.5 eV in μ_O°. Hence, this also yields an error of 0.5 eV in the formation energy of for instance $v_O^{\bullet\bullet}$ as this quantity is proportional to μ_O. Other molecules are on the other hand described better; the binding energies of H_2O and H_2 are off by merely ~50 meV [38, 39]. Hence, at finite temperatures (and partial pressures) the error introduced through μ_O° can be circumvented by assuming an equilibrium gas mixture of $H_2(g) + \frac{1}{2}O_2(g) = H_2O(g)$, in which:

$$\mu_O(T,P) + 2\mu_H(T,P) = \mu_{H_2O}(T,P) \quad (14)$$

where μ_{H} and $\mu_{\mathrm{H_2O}}$ are given by Eq. 7 and their equilibrium partial pressures. One thus avoids the use of μ_{O}° and the errors therein, a strategy adopted throughout this thesis.

Finite size effects

Modeling point defects in periodically repeating, limited sized supercells is inherently intricate due to lattice relaxations around the defects, charge compensation by a jellium background, and Coulombic interactions between a charged defect and its neighboring image, which all affect the calculated defect formation energies. One should thus in principle choose a sufficient supercell size to avoid such interactions. However, this limit in many cases corresponds to several hundred or thousands of atoms [23], which can be reached in LDA/PBE calculations, but is far too expensive if employing for instance hybrid functionals, or even worse, quasiparticle calculations (G_0W_0). Various authors have applied various *post* corrections to extrapolate defect formation energies to the infinite dilution limit by calculating the defects' formation energies in range of supercell sizes (see for instance Oba *et al.* [23]). However, defects in real systems tend also to affect each other and one may wonder whether the formation energy calculated using such an approach represents the defects' formation energy in a real system with a small, but finite defect concentration. As such, in Paper 5 we adopted an alternative strategy; the HSE obtained formation energies (using a 72 atoms supercell) were extrapolated to those in a 576 atoms supercell by using the defects' supercell size dependence from PBE calculations. The corrections from the 72 to 576 atoms supercell are fairly large, and amount to -0.61 eV and -0.15 for $v_O^{\bullet\bullet}$ and $OH_O^{\bullet}$, respectively. Similarly, in the case of the pyrochlore $Sm_2Zr_2O_7$ from Paper 3, the formation energy change from a 88 atoms (1×1×1) to a 704 atoms supercell (2×2×2 unit cells) amounts to -0.28 and -0.03 eV for $v_O^{\bullet\bullet}$ and $OH_O^{\bullet}$, respectively. This error is thus material dependent and depends on the extent of defect induced relaxations, charge of the defect, and dielectric constant of the material, and should be checked carefully in each situation.

Non-ground state structures

A pitfall encountered throughout this thesis deals with modeling of non-ground state structures, or local minima on the global potential energy surface of a compound. In all DFT codes, the user is free to define the crystal structure of the system, that being the ground state (0 K) structure (global minimum) or a high temperature polymorph (local minimum), and the system is relaxed to the closest minimum. While this usually poses no problems when modeling perfect systems, introducing a symmetry breaking defect in the lattice may have large effects on relaxation of the system. Starting from a high temperature local minimum structure, the forces acting on for instance the oxide ions neighboring an aperiodicity, such as a protonic defect, may induce long range periodic displacements of the oxide ions throughout the crystal lattice, and thus induce relaxation of the entire crystal towards the ground state minimum. As experienced in this thesis, this is most problematic for polymorphs that are

separated by minor ionic displacements, or in other words, where the activation energy for transformation between the polymorphs is small. For instance the perovskites $SrZrO_3$, $CaZrO_3$ and $PbZrO_3$ all crystallize in the cubic Pm-3m structure at higher temperatures and lower symmetric orthorhombic structures in the ground state. A proton or oxygen vacancy introduced in the cubic Pm-3m supercell results in splitting of the oxygen positions due to tilting of the ZrO_6 polyhedra, and the relaxed defective structures resemble the orthorhombic ground state (see Figure 5). Hence, a defect's formation energy calculated in the local minimum polymorph is highly uncertain since it inevitably contains a stabilizing contribution due to relaxations between the two polymorphs. In many cases such relaxations may be avoided by choosing a finer relaxation algorithm or smaller step lengths, a large supercell or supercell of a given periodicity. Similarly, $BaZrO_3$ and $SrTiO_3$ are often thought to be cubic perovskites, but both display lower symmetric ground state structures [40, 41], and long range relaxations upon introduction of defects were observed in both cases in this thesis. For $BaZrO_3$, the relaxations were avoided by using fine relaxations (and also a larger supercell with a periodicity of 2× the unit cell), while $SrTiO_3$ displayed large relaxations regardless of the relaxations technique. In that respect, a specific publication by Bork *et al*.[42] on cubic $SrTiO_3$ should be mentioned. The publication presents DFT calculations indicating that two $OH_O^{\bullet}$ defects on nearest neighbor O ions with parallel O-H axes are more stable than the two defects on distant O ions, due to stabilizing relaxations of the former configuration. The authors interpret this as a 'dihydrogen' complex, and also claim that protons thus may diffuse in a correlated pair-wise manner in oxides. However, another possible explanation is that two parallel $OH_O^{\bullet}$ defects in the cubic $SrTiO_3$ structure have a larger tendency to displace the entire system towards the ground state structure than two distant (or antiparallel) $OH_O^{\bullet}$ defects. In that respect, test calculations on $SrTiO_3$ in this thesis using three supercells consisting of 2×2×2, 3×3×3 or 4×4×4 unit cells, indicate that the stabilization of the hydrogen pair decreases with increasing supercell size, and diminishes in the largest supercell. Hence, such reports should be judged critically, and it is import to evaluate the physical relevance of defect induced relaxations in such structures.

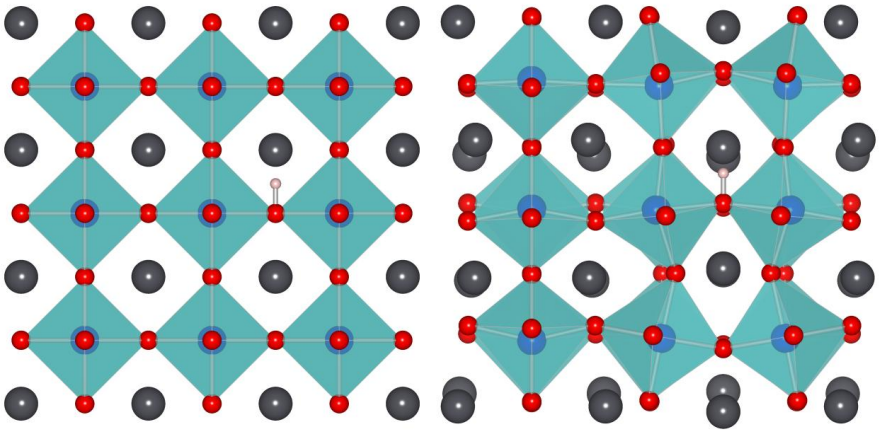

Figure 5: Protons in a 3×3×3 cubic supercell of $PbZrO_3$. The left figure shows the unrelaxed structure, while the right figure shows the fully relaxed structure reflecting the long range relaxations due to the protonic defect.

3. Papers

I. **A combined conductivity and DFT study of protons in $PbZrO_3$ and alkaline earth zirconate perovskites**, T. S. Bjørheim, A. Kuwabara, I. Ahmed, R. Haugsrud, S. Stølen and T. Norby, *Solid State Ionics*, **181**, 2010, 130.

II. **Hydration and proton conductivity in $LaAsO_4$**, T. S. Bjørheim, T. Norby and R. Haugsrud, *Journal of Materials Chemistry*, **22**, 2012, 1652.

III. **Hydration thermodynamics of pyrochlore structured oxides from TG and first principles calculations**, T. S. Bjørheim, V. Besikiotis and R. Haugsrud, *Dalton Transactions*, **41**, 2012, 13343

IV. **Hydration of Rutile TiO_2: Thermodynamics and Effects on n- and p-Type Electronic Conduction**, S. Erdal, C. Kongshaug, T. S. Bjørheim, N. Jalarvo, R. Haugsrud and T. Norby, *Journal of Physical Chemistry C*, **114**, 2010, 9139.

V. **Defect chemistry of rutile TiO_2 from first principles calculations**, T. S. Bjørheim, A. Kuwabara and T. Norby, Submitted, *Journal of Physical Chemistry C*, 2012.

VI. **Defects at the (1 1 0) surface of rutile TiO_2 from ab initio calculations**, T. S. Bjørheim, A. Kuwabara, C. E. Mohn and T. Norby, *International Journal of Hydrogen Energy*, **37**, 2012, 8110.

VII. **H and Li related defects in ZnO and their effect on electrical properties**, T. S. Bjørheim, S. Erdal, K. M. Johansen, K. E. Knutsen and T. Norby, *Journal of Physical Chemistry C*, 2012, 10.1021/jp307835c.

Paper 1

A combined conductivity and DFT study of protons in $PbZrO_3$ and alkaline earth zirconate perovskites,
T. S. Bjørheim, A. Kuwabara, I. Ahmed, R. Haugsrud, S. Stølen and T. Norby,
Solid State Ionics, **181**, 2010, 130

Paper 2

Hydration and proton conductivity in $LaAsO_4$,
T. S. Bjørheim, T. Norby and R. Haugsrud,
Journal of Materials Chemistry, **22**, 2012, 1652

Paper 3

Hydration thermodynamics of pyrochlore structured oxides from TG and first principles calculations,
T. S. Bjørheim, V. Besikiotis and R. Haugsrud,
Dalton Transactions, **41**, 2012, 13343

Erratum:
The correct form of Eq. 11 is

$$[\mathrm{OH}_{\mathrm{O}}^{\bullet}] = \frac{K_{\mathrm{hydr}}\left(N_{\mathrm{s,OH}_{\mathrm{O}}^{\bullet}} N_{\mathrm{c,OH}_{\mathrm{O}}^{\bullet}}\right)^2}{4 N_{\mathrm{s,v}_{\mathrm{O}}^{\bullet\bullet}} N_{\mathrm{c,v}_{\mathrm{O}}^{\bullet\bullet}}} \left(\frac{p_{\mathrm{H_2O}}}{p^{\circ}}\right) \left(-1 + \sqrt{1 + \frac{8 N_{\mathrm{s,v}_{\mathrm{O}}^{\bullet\bullet}} N_{\mathrm{c,v}_{\mathrm{O}}^{\bullet\bullet}} \left[\mathrm{Ca}_{\mathrm{RE}}^{/}\right]}{K_{\mathrm{hydr}}\left(N_{\mathrm{s,OH}_{\mathrm{O}}^{\bullet}} N_{\mathrm{c,OH}_{\mathrm{O}}^{\bullet}}\right)^2 \left(\frac{p_{\mathrm{H_2O}}}{p^{\circ}}\right)}} \right)$$

Paper 4

Hydration of Rutile TiO_2: Thermodynamics and Effects on n- and p-Type Electronic Conduction,
S. Erdal, C. Kongshaug, T. S. Bjørheim, N. Jalarvo, R. Haugsrud and T. Norby,
Journal of Physical Chemistry C, **114,** 2010, 9139

Paper 5

Defect chemistry of rutile TiO_2 from first principles calculations,
T. S. Bjørheim, A. Kuwabara and T. Norby,
Journal of Physical Chemistry C, 2012

Paper 6

Defects at the (1 1 0) surface of rutile TiO_2 from ab initio calculations,
T. S. Bjørheim, A. Kuwabara, C. E. Mohn and T. Norby,
International Journal of Hydrogen Energy, **37**, 2012, 8110

Paper 7

H and Li related defects in ZnO and their effect on electrical properties,
T. S. Bjørheim, S. Erdal, K. M. Johansen, K. E. Knutsen and T. Norby,
Journal of Physical Chemistry C, 2012, 10.1021/jp307835c

4. Discussion

The papers included in this thesis cover a wide range of oxides with different functional properties, and I will in the following discussion therefore elaborate on more general topics encountered in the papers. The first part of this discussion is dedicated to the general behavior of hydrogen in oxides, its possible charge states and aspects related to the hydration thermodynamics of various oxide classes. The second part is dedicated to association of hydrogen with cation vacancies and aliovalent acceptors, with selected examples on how such complexes may dominate the low temperature defect chemistry of functional oxides.

4.1 Hydrogen in oxides

Hydrogen species in oxides

Hydrogen may take in a variety of positions and effective charge states in oxides. The most commonly encountered species is the protonic defect, which usually occupies interstitial sites close to the oxide ions in the form of hydroxide defects, OH_O^q. This is illustrated by the potential energy surface of a single proton (H^+) in TiO_2 as obtained from DFT [43] in Figure 6 (left), where the red regions that signify its stability regime are found in the vicinity of the O ions.

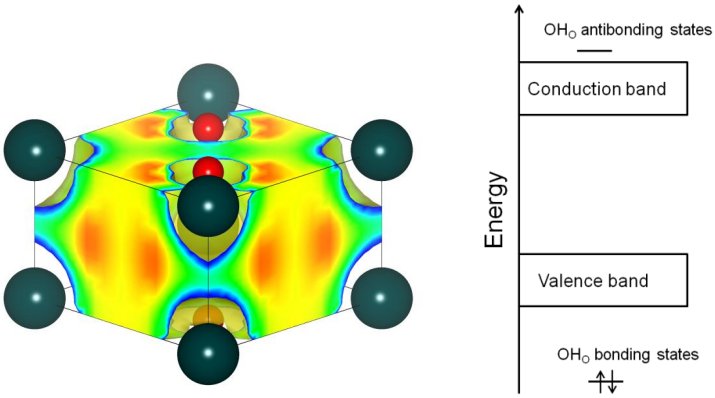

Figure 6: Left: calculated potential energy surface of a single H^+ defect in rutile TiO_2 from ref. [43]. The red regions signify its stabile regions and are found close to the oxide ions, and the defect is better described as a hydroxide defect, $OH_O^\bullet$. Right: schematic representation of the defect's bonding and antibonding state with respect to the band edges, reflecting its shallow donor behavior.

The bonding and antibonding states of this defect usually appear below the valence band and above the conduction band, respectively, as sketched in Figure 6 (right). Hence, addition of an electron to $OH_O^{\bullet}$ results in the electron being donated to the conduction band. $OH_O^{\times}$ is thus termed a shallow donor and exclusively exists as the effectively positive $OH_O^{\bullet}$ defect.

Although the pure interstitial H positions close to the cations are high in energy in the dense rutile structure (Figure 6), H may take on such positions in more open structures. This may be illustrated by for instance a H^- defect in the perovskite $PbZrO_3$ (see Figure 7). The H^- is found at a pure interstitial site between the Pb ions, and the corresponding partial charge density of the H1s state is primarily localized on H itself. Further, the H1s state falls close to the valence band (see Figure 7), and the two electrons of H^- are thus associated with the H1s orbital. Hence, H behaves almost as a purely interstitial hydride ion in such positions, or a $H_i^{/}$ defect. The relative stability of $OH_O^{\bullet}$ and $H_i^{/}$ and thus the possible existence of the latter (*i.e.,* the thermodynamic transition level between the two charge states, (+/-)), depends both on the structure, elemental composition and electronic structure of the oxide, and Neugebauer and Van de Walle correlated this level to the position of a materials' band edges with respect to the vacuum level [12].

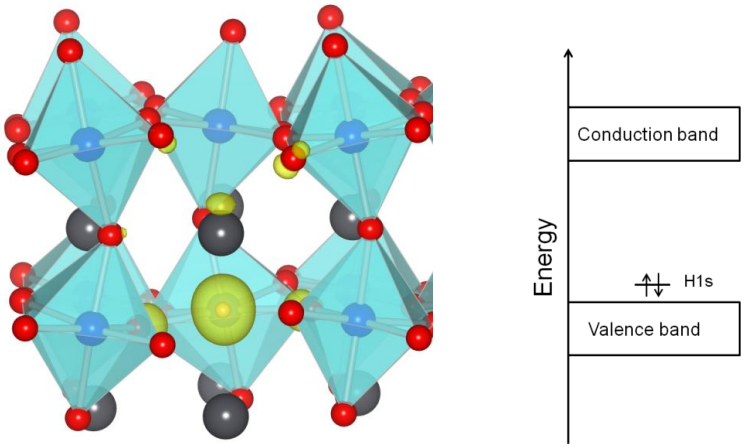

Figure 7: Left: H^- in orthorhombic $PbZrO_3$ with isosurfaces of the wave functions associated with the H1s bonding state, indicating that the defect is a pure interstitial hydride ion, $H_i^{/}$. Right: schematic band diagram indicating the position of the occupied H1s state, with respect to the band edges.

In oxides with more covalent units, H may interact with larger parts of the crystal. For instance in $LaAsO_4$, which is built from covalent AsO_4 units, we showed in Paper 2 that the defect level associated with a $OH_O^{\bullet}$ defect spreads over an entire AsO_4 unit. The $OH_O^{\bullet}$ defect is in this material therefore better described as a substitutional hydrogen arsenate ion, $(HAsO_4)_{AsO4}^{\bullet}$.

Hydrogen may also substitute an oxide ion in the form of H_O^q defects. In such positions, H hybridizes and bonds to the surrounding cations, and is therefore often termed 'multicentred' H [17]. The H_O^q defect is a shallow donor and ionizes to the effectively positive $H_O^\bullet$ defect [17]. However, H itself must accommodate an electron and is therefore by all means a hydride ion in such positions.

Although hydrogen may take on various positions and charge states in oxides, its dominating form depends both on the relative formation energies of the possible H defects, and also on the formation energies or concentrations of all other defects. As such, the dominating H defect in an oxide is strongly dependent on temperature and atmospheric conditions. This is illustrated by the p_{O_2} dependencies of the defect concentrations in rutile TiO_2 (Paper 5) and ZnO (Paper 7) at 1000 and 900 K, respectively, as obtained from DFT calculations (Figure 8). Under moderately reducing conditions, both materials dissolve protons through compensation by electrons with the electroneutrality given by $[OH_O^\bullet] = n \propto p_{O_2}^{-1/8} p_{H_2O}^{1/4}$. The concentration of substitutional hydride ions, $H_O^\bullet$, is in minority with respect to protonic defects, $OH_O^\bullet$, in both materials, but increases with decreasing p_{O_2}. In TiO_2, $H_O^\bullet$ is in minority with respect to $OH_O^\bullet$ even under 1 atm H_2(g) at 1000 K. In ZnO however, $H_O^\bullet$ is more stable with respect to $OH_O^\bullet$ (and $v_O^{\bullet\bullet}$) and comes up as the dominating positive defect in the most reducing atmospheres, yielding the situation $[H_O^\bullet] = n \propto p_{O_2}^{-3/8} p_{H_2O}^{1/4}$. However, as shown in Paper 7, neither as-grown nor Li doped ZnO displays a $p_{O_2}^{-3/8}$ reminiscent dependency of the electron conductivity in diluted H_2(g) (at constant p_{H_2O}) at 600 °C. This could be due to various impurities present in as-grown ZnO, which thus are not captured by the calculations. Another possibility is that this discrepancy reflects computational inaccuracies which could shift the changeover temperature between two defect structures somewhat, and one might encounter such a $H_O^\bullet$ dominated defect chemistry only at higher temperatures.

The equilibrium concentrations of hydride ions ($H_O^\bullet$) in Figure 8 are small, but they may be increased significantly under even more reducing conditions by reduction with for instance CaH_2(s). There are several recent reports of successful preparation of oxides with compositional amounts of $H_O^\bullet$ in this manner, notably $LaSrCoO_3H_{0.7}$ [44, 45] and the perovskite structured $BaTiO_{3-x}H_x$ [46]. Similar as in ZnO, these oxides most likely display the defect structure $[H_O^\bullet] = n$, although with partial reduction of the multivalent cations. Hydridation of oxides in this manner may be described by for instance:

$$3H_2(g) + 2O_O^\times = 2H_O^\bullet + 2e' + 2H_2O(g) \qquad (15)$$

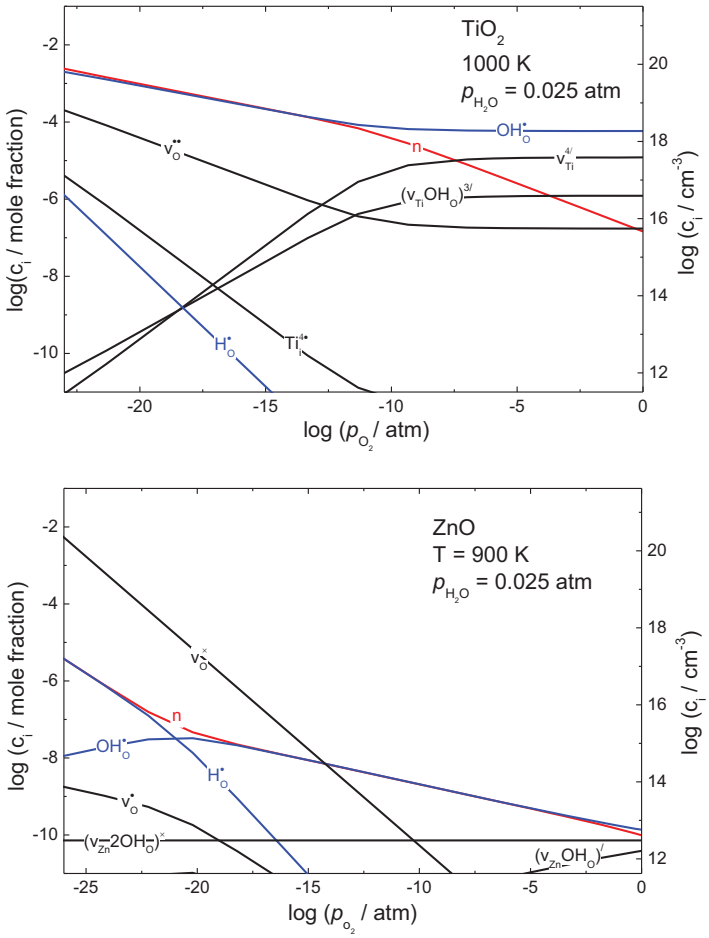

Figure 8: Equilibrium defect concentrations in TiO_2 and ZnO (from hybrid DFT calculations in Paper 5 and 7) as a function of p_{O_2} under wet conditions in the range from 1 atm O_2 to 1 atm H_2(g) at 1000 and 900 K, respectively.

for which the Gibbs energy clearly depends on the Fermi level, and thus the band gap of the oxide. One may thus expect hydridation according to Eq. 15 to be most pronounced in oxides with smaller band gaps.

In insulators with wider band gaps, other negative defects such as interstitial hydride ions, $H_i^{/}$, may in principle act as the charge-compensating defect. Figure 9 shows the equilibrium defect structure of cubic ZrO_2 from DFT calculations [1] by assuming an acceptor concentration of 0.08 mole fraction under reducing conditions. The $OH_O^{\bullet}/H_i^{/}$ transition level appears 2.1 eV

[1] In the DFT calculations of ZrO_2 I used a 96 atoms supercell of the cubic polymorph and the GGA-PBE functional, which yields an underestimated band gap of 3.6 eV. Electronic defects are for simplicity neglected when solving the electroneutrality in Figure 9.

above the valence band, and both defects may thus in principle dominate, depending on the Fermi level. Further, the calculated hydration enthalpy (according to Eq. 18) is positive, with the consequence that $OH_O^{\bullet}$ always is in minority with respect to $v_O^{\bullet\bullet}$, and $H_O^{\bullet}$ thus constitutes the dominating hydrogen defect in wet $H_2(g)$. Under even more reducing conditions, such as upon reduction with CaH_2, the concentration of $H_O^{\bullet}$ would ultimately surpass that of $v_O^{\bullet\bullet}$, yielding the electroneutrality $[H_O^{\bullet}] = \left[Y_{Zr}^{/}\right]$. Similarly, the calculations predict an even more exotic defect structure in undoped ZrO_2 upon reduction with CaH_2, notably $[H_O^{\bullet}] = \left[H_i^{/}\right]$, or self-compensating hydride ions.

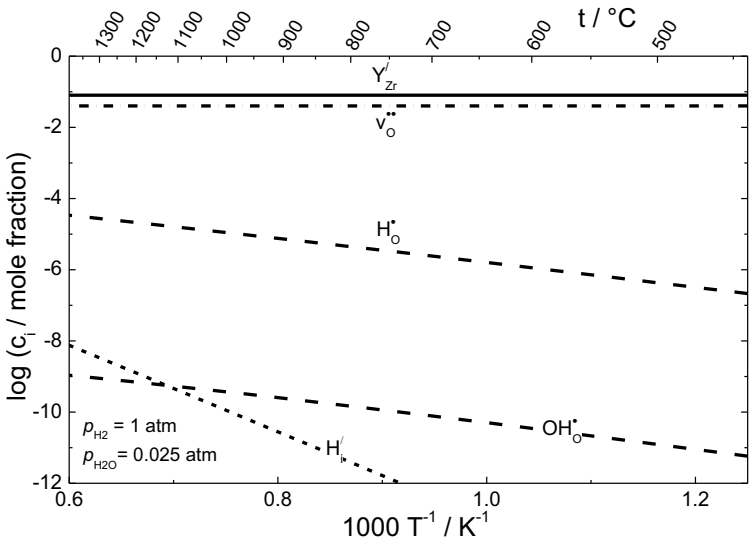

Figure 9: Equilibrium concentrations of selected ionic defects in cubic ZrO_2 under wet $H_2(g)$ as emerging from DFT calculations by assuming a Y concentration of 0.08 mole fraction.

Although such $H_O^{\bullet}$ defects only have been described in a handful of oxides in the last couple of years [14, 17, 44-48], and often are neglected in experimental investigations of defect related properties of oxides, there are indications that these defects are more important in oxides than previously assumed. Steinsvik *et al.* [13] observed an apparent change from positive to negative EMF for $SrTi_{1-x}Fe_xO_3$ in a hydrogen concentration cell under reducing conditions, interpreted as apparent transport of negative hydrogen species, which they speculated could be due to the $H_O^{\bullet}$ defect. A similar behavior has later been reported for a variety of oxides, for instance for Y-stabilized ZrO_2 [49]. Widerøe *et al.* [16] also suggested that a negative, or a neutral hydrogen defect, could be the reason for the observed negative transport number, although no definite experimental results supporting thus indication exists.

Janotti and Van de Walle [50] claimed $H_O^{\bullet}$ defects to be fairly immobile in ZnO based on a calculated dissociation enthalpy of 3.8 eV according to:

$$H_O^{\bullet} + O_O^{\times} = v_O^{\times} + OH_O^{\bullet} \quad (16)$$

and a mobility enthalpy of 2.8 eV through concerted exchange with a neighboring oxide ion. However, our more accurate hybrid-DFT calculations yielded a more modest enthalpy of 1.1 eV for Eq. 16 (see Paper 7), and $H_O^{\bullet}$ may, in principle, diffuse within the oxygen lattice by jumping as a proton, leaving behind a neutral oxygen vacancy. Even more likely, and especially in oxides with high concentrations of charged oxygen vacancies $v_O^{\bullet\bullet}$ such as YSZ (see Figure 9), is a process in which $H_O^{\bullet}$ jumps as a hydride ion to a neighboring $v_O^{\bullet\bullet}$ by leaving one $v_O^{\bullet\bullet}$ behind. $H_O^{\bullet}$ thus jumps within the oxygen lattice, and this process should in principle be comparable to that of O ions in the oxide. Such a mechanism could therefore in principle be the transport described as due to 'apparent hydride ion' or 'neutral hydrogen' species in solid state ionics research. Interestingly, such a diffusion process has been claimed to be at play in $LaSrCoO_3H_{0.7}$ [45] for which quasi-elastic neutron scattering indicated high hydride ion diffusivity, with a mobility enthalpy of 0.2-0.23 eV and estimated hydride ion conductivity of 3-5 S cm^{-1} at ~700 K. Hence, the estimated hydride ion conductivity is 2 orders of magnitude higher than the maximum proton conductivity of state-of-the-art proton conductors. Although such oxides could display record high ionic conductivities, their practical implementation is hindered by their poor stability in oxidizing atmospheres [46], and are therefore mostly an academic curiosity.

Hydrogen and electrons

As shown in Figure 8 (and Paper 5 and 7), oxides with moderate band gaps such as TiO_2 and ZnO, may display the electroneutrality $[OH_O^{\bullet}] = n$ under reducing conditions. The electrons may either be delocalized in the conduction band, or, as is likely in oxides with multivalent cations, localize on cations in the form of polaronic defects, or $M_M^{/}$. In that respect, it has been speculated whether such effectively negative polaronic defects may associate with positive point defects such as $OH_O^{\bullet}$ (see Paper 5). Figure 10 displays the relaxed configuration of a $OH_O^{\bullet}$ defect with one (left) and two (right) electrons in the same supercell for rutile TiO_2 (top) and Cr_2O_3 [2] (bottom) with the partial charge densities of the resulting in-gap defect state(s). For TiO_2, the charge densities are mainly spread over Ti ions distant from the $OH_O^{\bullet}$ in both cases. This indicates that the association of the two defects is fairly weak and is overshadowed by defect-defect interactions due to the limited size of the employed supercells. For Cr_2O_3 however, both $OH_O^{\bullet} + e^{/}$ and $OH_O^{\bullet} + 2e^{/}$ resulted in a ground state with the electrons localized on Cr ions coordinated to the $OH_O^{\bullet}$ defect, indicative of a significant association. The binding enthalpies of $(OH_O Cr_{Cr})^{\times}$ and $(OH_O 2Cr_{Cr})^{/}$ may be quantified from the formation energy difference between the complexes, and $OH_O^{\bullet}$ and delocalized conduction band electrons, and amount to 0.61 and 0.73 eV, respectively. The binding per electron is thus

[2] For Cr_2O_3 I employed hybrid DFT calculations using the HSE functional intermixing 13 % HF exchange and a 120 atoms supercell. All calculations were performed with an antiferromagnetic ordering of the Cr^{3+} ions.

strongest for the $(OH_O Cr_{Cr})^{\times}$ complex, while the structural relaxations in $(OH_O 2Cr_{Cr})^{/}$ counteract the energy gain from trapping of the second electron. Hence, the OH_O^q ($q = 0$) defect is by all means a shallow donor and is effectively positive in both TiO_2 and Cr_2O_3, but they may in such and similar 3d transition metal oxides trap electrons in proton-polaron complexes. Further, given the relatively strong binding energy of this complex in certain oxides, the two defects could in principle diffuse through a correlated jump mechanism, and there is thus nothing preventing a diffusing proton from dragging along an electron on its way through such oxides. Despite extensive test calculations throughout this thesis, similar proton-polaron complexes were not observed in any of the other included oxides, notably ZrO_2, ZnO, $PbZrO_3$ or $LaAsO_4$. Nevertheless, one may expect such complexes to be important in especially Cr, Fe, V and to some extent Ti containing compounds such as $LaCrO_3$, Fe_2O_3 and $BaTiO_3$ under reducing conditions. These complexes could also in principle be the explanation for the transport of apparent neutral or negative hydrogen species under reducing conditions as discussed in the previous section.

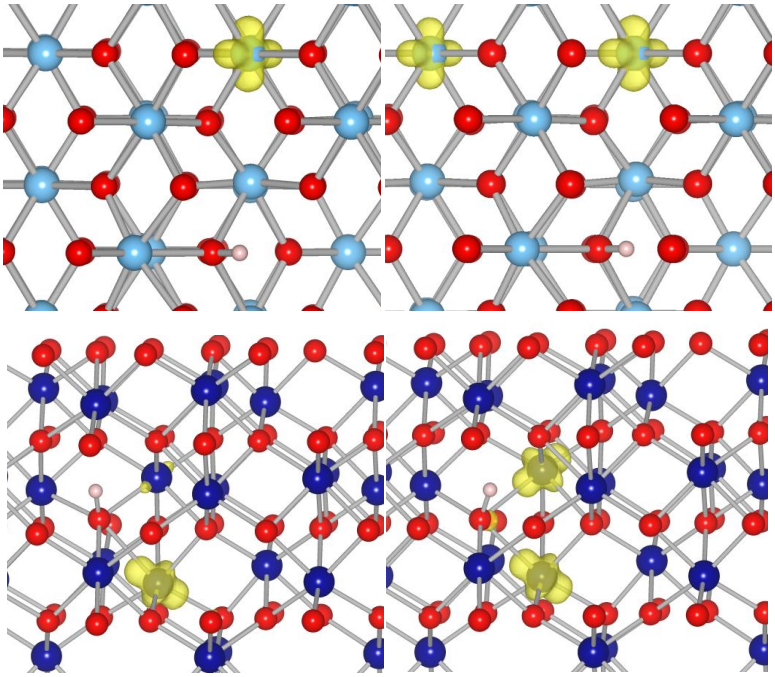

Figure 10: Relaxed configurations of $OH_O^{\bullet} + e^{/}$ (left) and $OH_O^{\bullet} + 2e^{/}$ (right) in rutile TiO_2 (top) and Cr_2O_3 (bottom) with partial charge densities of the defect state(s). See Paper 5 and footnote 2 for computational details.

Hydration thermodynamics

Acceptor doped, wide band gap and insulating oxides are to a large extent found to display the electroneutrality (see Paper 1-5):

$$\left[\mathrm{A}^{/}\right] = 2[\mathrm{v}_{\mathrm{O}}^{\bullet\bullet}] + [\mathrm{OH}_{\mathrm{O}}^{\bullet}] \tag{17}$$

For oxides that display this electroneutrality, dissolution of protons is described by the equilibrium:

$$\mathrm{H_2O(g)} + \mathrm{v}_{\mathrm{O}}^{\bullet\bullet} + \mathrm{O}_{\mathrm{O}}^{\times} = 2\mathrm{OH}_{\mathrm{O}}^{\bullet} \tag{18}$$

The different contributions to the Gibbs energy of Eq. 18, $\Delta G^{\circ}_{\mathrm{hydr}}$, and their dependence on various materials parameters, has been debated in the literature since the discovery of proton conduction (*cf.* ref. [15, 51, 52]). To shed light on the different contributions, $\Delta G^{\circ}_{\mathrm{hydr}}$ may be split into electronic and vibrational contributions (see Section 2.4):

$$\Delta G^{\circ}_{\mathrm{hydr}} = \Delta G^{\mathrm{electronic}}_{\mathrm{hydr}} + \Delta G^{\mathrm{vibr,gas}}_{\mathrm{hydr}} + \Delta G^{\mathrm{vibr,solid}}_{\mathrm{hydr}} \tag{19}$$

$\Delta G^{\mathrm{electronic}}_{\mathrm{hydr}}$ is given by the change in electronic (or binding) energy upon hydration and may be obtained from for instance the 0 K formation energies of $\mathrm{OH}_{\mathrm{O}}^{\bullet}$ and $\mathrm{v}_{\mathrm{O}}^{\bullet\bullet}$:

$$\Delta G^{\mathrm{electronic}}_{\mathrm{hydr}} = 2\Delta H^{\mathrm{f,electronic}}_{\mathrm{OH}_{\mathrm{O}}^{\bullet}} - \Delta H^{\mathrm{f,electronic}}_{\mathrm{v}_{\mathrm{O}}^{\bullet\bullet}} = \Delta H^{\mathrm{electronic}}_{\mathrm{hydr}} \tag{20}$$

$\Delta G^{\mathrm{vibr,gas}}_{\mathrm{hydr}}$ is given by the zero-point energy of H_2O(g) and the temperature dependency of the chemical potential of H_2O(g), $\mu_{\mathrm{H_2O}}(T, p^{\circ})$ (Eq. 7):

$$\Delta G^{\mathrm{vibr,gas}}_{\mathrm{hydr}} = -\left[\sum_{i=1}^{3} \frac{\mathrm{h}\nu_{i,\mathrm{H_2O}}}{2} + H_{\mathrm{H_2O}}(T, p^{\circ}) - S_{\mathrm{H_2O}}(T, p^{\circ})\right] \tag{21}$$

Finally, $\Delta G^{\mathrm{vibr,solid}}_{\mathrm{hydr}}$ is given by changes in the vibrational properties of the crystal upon defect formation/consumption (see Chapter 2). $\Delta G^{\mathrm{vibr,solid}}_{\mathrm{hydr}}$ may thus be approximated by the free energy of the 6 O-H related modes (two $\mathrm{OH}_{\mathrm{O}}^{\bullet}$ defects) and the 3 O modes (filling of a $\mathrm{v}_{\mathrm{O}}^{\bullet\bullet}$) formed upon hydration, and the contribution due to changes in the vibrational modes of the $j \epsilon [1, N]$ neighboring ions:

$$\begin{aligned}
&\Delta G^{\mathrm{vibr,solid}}_{\mathrm{hydr}} = \\
&2\left[\sum_{i=1}^{3}\left\{\frac{h\nu_{i,\mathrm{OH}_{\mathrm{O}}^{\bullet}}}{2} + k_{\mathrm{b}}T\ln[1-\exp(-\frac{h\nu_{i,\mathrm{OH}_{\mathrm{O}}^{\bullet}}}{k_{\mathrm{b}}T})]\right\} + \sum_{j=1}^{N}\left\{\frac{h(\nu_{j,\mathrm{OH}_{\mathrm{O}}^{\bullet}}-\nu_{j,\mathrm{bulk}})}{2} + k_{\mathrm{b}}T\ln\frac{1-\exp(-\frac{h\nu_{j,\mathrm{OH}_{\mathrm{O}}^{\bullet}}}{k_{\mathrm{b}}T})}{1-\exp(-\frac{h\nu_{j,\mathrm{bulk}}}{k_{\mathrm{b}}T})}\right\}\right] + \\
&\sum_{i=1}^{3}\left\{\frac{h\nu_{i,\nu_{i,\mathrm{O}_{\mathrm{O}}^{\times}}}}{2} + k_{\mathrm{b}}T\ln[1-\exp(-\frac{h\nu_{i,\nu_{i,\mathrm{O}_{\mathrm{O}}^{\times}}}}{k_{\mathrm{b}}T})]\right\} + \sum_{j=1}^{N}\left\{\frac{h(\nu_{j,\mathrm{bulk}}-\nu_{j,\mathrm{v}_{\mathrm{O}}^{\bullet\bullet}})}{2} + k_{\mathrm{b}}T\ln\frac{1-\exp(-\frac{h\nu_{j,\mathrm{bulk}}}{k_{\mathrm{b}}T})}{1-\exp(-\frac{h\nu_{j,\mathrm{v}_{\mathrm{O}}^{\bullet\bullet}}}{k_{\mathrm{b}}T})}\right\}
\end{aligned} \tag{22}$$

Hence, the enthalpy part of $\Delta G^{\circ}_{\mathrm{hydr}}$ encompasses both the electronic hydration enthalpy (*i.e.*, the DFT obtained hydration enthalpies which are reported in Paper 1-5) and the zero point contributions from H_2O(g) and the additional lattice modes. The entropy part is composed of

the entropy of $H_2O(g)$ and the entropy change of the system due to creation/extinction of lattice modes. In Paper 3, we applied this simplified model to a selected series of pyrochlore oxides. Figure 11 displays $\Delta G^{\circ}_{\mathrm{hydr}}$ for $La_2Sn_2O_7$ by inclusion of various contributions in Eq. 19;

1. assuming contributions from only $\Delta H^{\mathrm{electronic}}_{\mathrm{hydr}}$ and $\mu_{\mathrm{H_2O}}(T, p^{\circ})$
2. + the 6 $OH^{\bullet}_{O}$ related modes and zero-point contributions of $OH^{\bullet}_{O}$ and $H_2O(g)$
3. + 3 bulk O related modes
4. + changes in the 16 nearest ions upon $OH^{\bullet}_{O}$ formation and $v^{\bullet\bullet}_{O}$ consumption, and accounting for collective modes.

The average $\Delta H^{\circ}_{\mathrm{hydr}}$ and $\Delta S^{\circ}_{\mathrm{hydr}}$ as obtained by linearizing the high temperature part of $\Delta G^{\circ}_{\mathrm{hydr}}$ are shown in Table 1. Although $\Delta S^{\circ}_{\mathrm{hydr}}$ has been claimed mostly to be due to loss of $H_2O(g)$, we note that the $\Delta S^{\circ}_{\mathrm{hydr}}$ in case 1 amounts to -215 J $K^{-1}mol^{-1}$, which is significantly more negative than the average -120±40 J $K^{-1}mol^{-1}$ found experimentally [15]. Inclusion of the O-H vibrational modes (case 2) increases the entropy somewhat, however, the most dominant

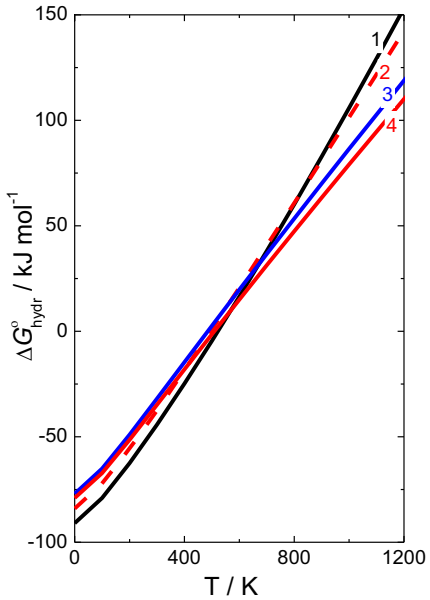

	$\Delta H^{\circ}_{\mathrm{hydr}}$ kJ mol^{-1}	$\Delta S^{\circ}_{\mathrm{hydr}}$ J K^{-1}mol^{-1}
Case 1	-109	-215
Case 2	-96	-198
Case 3	-81	-167
Case 4	-82	-161

Figure 11 and Table 1: $\Delta G^{\circ}_{\mathrm{hydr}}$ for $La_2Sn_2O_7$ from DFT and thermodynamic modeling by (case 1) including only $\Delta H^{\mathrm{electronic}}_{\mathrm{hydr}}$ and the temperature dependency of $\mu_{\mathrm{H_2O}}$, (case 2) addition of the contributions from the 6 $OH^{\bullet}_{O}$ modes and the zero-point energy of $H_2O(g)$ and (case 3) addition of the 3 O related modes, and (case 4) accounting for changes in the 16 nearest ions and collective modes.

effect is inclusion of the additional lattice O modes which corresponds to filling of the $v_O^{\bullet\bullet}$ (case 3). Hence, the high frequency O-H modes mostly contribute to the zero-point energy, while the low frequency O modes to a larger extent contribute to the temperature dependency of $\Delta G^{\circ}_{\mathrm{hydr}}$, as expected from Eq. 22. Finally, by accounting for changes in the vibrational modes of nearby ions and collective modes in the phonon calculations (case 4) the entropy increases only slightly compared to case 3. The error due to neglection of these contributions is thus small, at least within the pyrochlore series of oxides. However, these contributions can be more significant in other oxides, such as in the $REXO_4$ (RE = La-Lu, X = P, As, V and Nb) series where the oxygen vacancy induces larger structural relaxations (see Paper 2).

Figure 12 displays the calculated $\Delta G^{\circ}_{\mathrm{hydr}}$ for selected $RE_2X_2O_7$ pyrochlores by including the contributions listed in case 3 with the vibrational frequencies from Paper 3. The similar slopes for the different compositions reflect that the obtained $\Delta S^{\circ}_{\mathrm{hydr}}$ all fall in the range -165 to -170 J $K^{-1}mol^{-1}$, while there is a more notable change in $\Delta H^{\circ}_{\mathrm{hydr}}$ through the series. As shown in Paper 3, the $\Delta H^{\circ}_{\mathrm{hydr}}$ is slightly less negative than $\Delta H^{\mathrm{electronic}}_{\mathrm{hydr}}$, however, the change is similar for all compositions. The minor changes in $\Delta S^{\circ}_{\mathrm{hydr}}$ through the series reflect the only modest change in the vibrational frequencies due to the structural similarities through the series. As the bonding environment of $OH_O^{\bullet}$ is similar for a large variety of oxides, the O-H vibration modes are usually found in the range 700-1000 cm^{-1} and 3000-3600 cm^{-1} [53], and their contribution to $\Delta G^{\circ}_{\mathrm{hydr}}$ may thus be expected to be similar for a large variety of oxides. The cation-oxygen bonds may however change more with large structural changes, and the O modes and their contribution to $\Delta G^{\circ}_{\mathrm{hydr}}$ may thus change more between structurally different

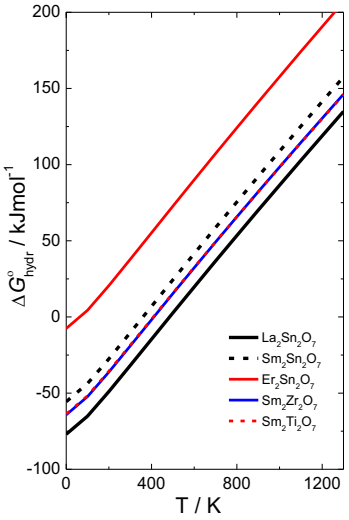

Figure 12: $\Delta G^{\circ}_{\mathrm{hydr}}$ for selected $RE_2X_2O_7$ pyrochlores from DFT and thermodynamic modeling according to Eq. 19, and case 3.

oxides (for instance from pyrochlore to monazite structured oxides). Nevertheless, the preceding discussion indicates that trends in the hydration thermodynamics of oxides largely are determined by changes in $\Delta H^{\circ}_{\mathrm{hydr}}$, or more precisely its electronic part, $\Delta H^{\mathrm{electronic}}_{\mathrm{hydr}}$, which will be elaborated on in later sections.

Configurational contributions

The large deviation between the experimentally obtained $\Delta S^{\circ}_{\mathrm{hydr}}$ (-120±40 J $K^{-1}mol^{-1}$ [15]), and those obtained from vibrational thermodynamics in this work (-165 to -170 J $K^{-1}mol^{-1}$), could arise from approximations used to extract the experimental values, or the simplification in the theoretical model. In Paper 2, we pointed out the significance of accounting for the configurational degeneracy of a defect, when applying a defect model to experimental results. More precisely, neglecting the number of configurations a defect may attain at each site in the equilibrium constant for the hydration reaction, yields a configurational contribution in the determined $\Delta S^{\circ}_{\mathrm{hydr}}$. In general, if defining the concentration of sites to that of bulk oxygen ions, the configurational part of the extracted hydration entropy amounts to $R\ln\left(\frac{N^2_{\mathrm{c,H}}}{\mathrm{N_{c,v_O}}}\right)$, where $N_{\mathrm{c,H}}$ and $N_{\mathrm{c,v_O}}$ are the number of configurations protons and oxygen vacancies, respectively, may attain at each regular defect site. While this usually equals 1 for oxygen vacancies, protons may attain various configurations depending on the symmetry and structure of the oxide. For instance, in the case of $BaZrO_3$ (cubic perovskite structure), with an experimental hydration entropy reported in the range -90 to -125 J $K^{-1}mol^{-1}$ [54], there are 4 possible configurations of a proton per O ion, and $N_{\mathrm{c,H}}$ = 4. Hence, the configurational part of the extracted hydration entropy amounts to +23 J $K^{-1}mol^{-1}$, and the entropy thus appears higher (less negative) than the entropy obtained when accounting for the configuration degeneracy.

Nevertheless, the hydration entropy of $BaZrO_3$ still deviates somewhat from the theoretical values presented here and by Björketun *et al.*[33] using a similar model (-174 J $K^{-1}mol^{-1}$). One may therefore suspect that additional contributions may have been neglected either in the experimental or theoretical models, for instance the effect of acceptor dopants. An acceptor dopant may change the number of possible proton and/or oxygen vacancy configurations, either through structural relaxations or by complex formation with protons or oxygen vacancies. For instance in the case of $BaZrO_3$, it has been indicated experimentally that the hydration entropy varies both with the type of dopant, and its concentration [54]. Tauer *et al.* [55] recently addressed this theoretically for the $BaCeO_3$ system. By accounting for the configurational entropy of the hydrated and unhydrated systems, they reported that the calculated overall hydration entropy increased (became less negative) with decreasing acceptor concentration. Although the applied methodology can be discussed, this indicates that such effects could explain the 'missing' contributions to the hydration entropy.

Hydration enthalpy trends

Over the last decade, several authors have speculated about possible correlations between ΔH°_{hydr} and various materials specific parameters [15, 51-53, 56, 57], which is also the focus of Paper 1 and 3. Figure 13 shows updated versions of the correlation plots in Paper 1, in which I have included DFT obtained hydration enthalpies (*i.e.*, $\Delta H^{electronic}_{hydr}$) of AXO_3 (A = Ba, Sr and X = Ti, Zr and Ce), $PbZrO_3$, $CaZrO_3$, and $LaXO_3$ (X = Al, In, Sc, Y, Er and Lu), in addition to the DFT obtained hydration enthalpies for the $RE_2X_2O_7$ pyrochlore series from Paper 3.

For perovskites, the enthalpy to some extent correlates with both the electronegativity difference (ΔX) and the tolerance factor. However, the scatter is large in both plots, especially for the experimental values, where the largest deviations are the enthalpies of $La_{0.9}Sr_{0.1}YO_3$ ($\Delta X = 0.04$ and ΔH°_{hydr} = -56 kJ mol^{-1}) and $SrZr_{0.95}Yb_{0.05}O_3$ ($\Delta X = 0.22$ and ΔH°_{hydr} = -147 kJ mol^{-1}). In addition, the enthalpies of the mixed perovskites $Ba_3(Ca_{1+x}Nb_{2-x})O_{9-\delta}$ (ΔX = 0.18 to 0.19 and ΔH°_{hydr} = -108 to -57 kJ mol^{-1}) deviate notably with the overall correlation. The overall fit of the two correlations is poor also for the DFT obtained values, where the most pronounced deviant is $LaInO_3$. Although these deviations partly may be explained by experimental and computational inaccuracies, they may also reflect that such correlations only apply to chemically and structurally similar oxides. The latter argument is supported by that, for the DFT obtained values, the regression lines of for instance each A site cation series,

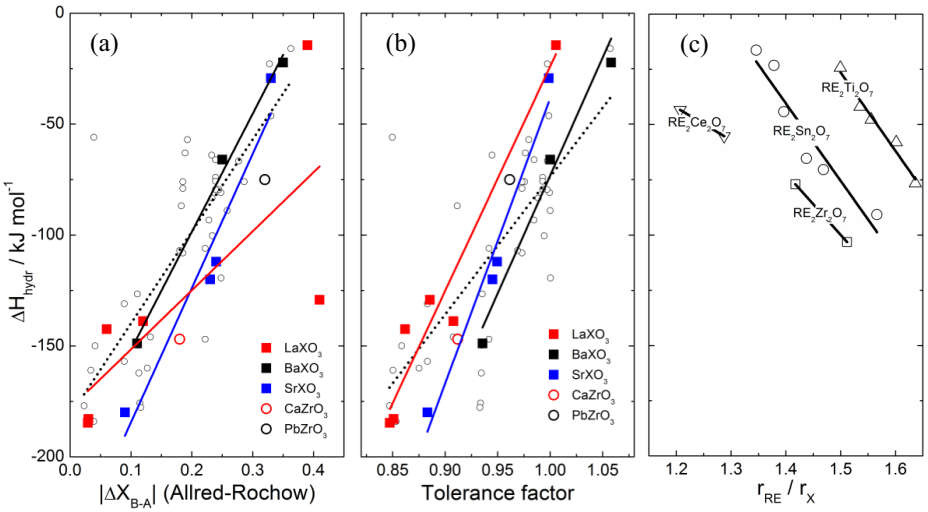

Figure 13: (a) and (b) hydration enthalpies of AXO_3 perovskites as a function of difference in electronegativity between the two cations, and tolerance factor. The small open symbols are experimental values from ref. [15] and larger symbols and their regression lines are the DFT values of the series $LaXO_3$ (X = Sc, Y, Er, Lu, Al and In), $BaXO_3$ and $SrXO_3$ (X = Ti, Zr and Ce). (c) DFT obtained hydration enthalpies for $RE_2X_2O_7$ (RE = La-Lu, X = Ti, Sn, Zr and Ce) pyrochlores as a function of the radius ratio of the two cations.

AXO_3 (A = Sr, Ba and La), are less scattered than the overall regression line. Further, the fact that the enthalpies correlate with both the electronegativity difference and the tolerance factor indicates that both parameters affect the hydration properties. While the ΔX is related to a perovskite's basicity [15, 56], and thus possibly the bonding nature of the two cations, the tolerance factor reflects its deviation from the perfect cubic perovskite structure (*i.e.,* tetragonal, cubic or orthorhombic symmetry). The two parameters also correlate with each other and with the perovskites' formation enthalpy; the smaller the electronegativity difference and the lower the tolerance factor, the less exothermic is the formation enthalpy [37, 58, 59] and the more exothermic is the hydration enthalpy.

For the pyrochlores series, there is an obvious correlation between the radius ratio of the two cations and the hydration enthalpy within each X ion series; smaller RE ions result in less exothermic hydration enthalpies. Contrary to the perovskite oxides, the pyrochlore oxides retain a cubic symmetry for all compositions, and the trend may therefore be linked to changes in the bonding nature or stability of the oxides through the series. In Paper 3, we explained this trend by both destabilization of protons and stabilization of oxygen vacancies with decreasing RE ion size, which again was attributed to destabilization of the oxide and increasing degree of ionicity.

The most exothermic hydration enthalpies are in the pyrochlores found for the most stable oxides, which seemingly is opposite to the trend in the perovskite series. Within the rare-earth sesquioxides on the other hand, both the hydration enthalpy and the formation enthalpy decreases (more exothermic) with decreasing RE ion size [52, 57], and the most exothermic hydration enthalpies are thus found for the most stable oxides as in the pyrochlore series. Contrary to the perovskites, where both A and X seemingly affect the hydration enthalpy, there is only a minor effect of changing the X ion in the pyrochlores on their hydration enthalpy, as we also indicated for the $LaXO_4$ (X = V, As and P) monazite oxides in Paper 2. We speculate whether this could be due to counteracting contributions from stabilization of both protons and vacancies upon X ion substitution, which thus seemingly are structurally dependent. These observations indicate that the hydration enthalpy of oxides depends on both structure and symmetry, bonding nature and stability of the oxide itself, and the contribution from either parameter seems to differ between different structural classes, thus making judgment of general trends that apply to a large selection of oxides difficult.

Isotope effect on hydration thermodynamics

Isotope exchange measurements are often used as an indication of whether protons contribute to the overall conductivity (see for instance Paper 1, 2, 4 and 7). An often neglected effect of shifting between $H_2O(g)$ and $D_2O(g)$ is the possible effect on the standard hydration thermodynamics of the oxide, or the difference in the thermodynamics of:

$$H_2O(g) + v_O^{\bullet\bullet} + O_O^{\times} = 2OH_O^{\bullet} \quad (23)$$

$$D_2O(g) + v_O^{\bullet\bullet} + O_O^{\times} = 2OD_O^{\bullet} \quad (24)$$

Upon substitution of $H_2O(g)$ by $D_2O(g)$, clearly the chemical potential of the gas species changes, but also the vibrational modes $OH_O^{\bullet}$ and $OD_O^{\bullet}$ are different, thus resulting in changes in the solid state vibrational contributions to $\Delta G^{\circ}_{\mathrm{hydr}}$ (see Eq. 22). By assuming that the electronic stability of the two defects is identical, the $\Delta G^{\circ}_{\mathrm{hydr}}$ for Eq. 23 and 24 amounts to:

$$\Delta_{H_2O\rightarrow D_2O}(\Delta G^{\circ}_{\mathrm{hydr}}) = 2\left\{\sum_{i=1}^{3}\frac{h\nu_{i,OH_O^{\bullet}}}{2} + k_bT\ln[1-\exp(-\frac{h\nu_{i,OH_O^{\bullet}}}{k_bT})]\right\} - 2\left\{\sum_{i=1}^{3}\frac{h\nu_{i,OD_O^{\bullet}}}{2} + k_bT\ln[1-\exp(-\frac{h\nu_{i,OD_O^{\bullet}}}{k_bT})]\right\} - \left(\sum_{i=1}^{3}\frac{h\nu_{i,H_2O}}{2} - \sum_{i=1}^{3}\frac{h\nu_{i,D_2O}}{2}\right) - \left(\mu_{H_2O}(T,p^{\circ}) - \mu_{D_2O}(T,p^{\circ})\right) \quad (25)$$

There is thus a change in the zero-point contributions to $\Delta H^{\circ}_{\mathrm{hydr}}$ and both the gasous and solid state vibrational contributions to $\Delta S^{\circ}_{\mathrm{hydr}}$. Figure 14 displays $\Delta G^{\circ}_{\mathrm{hydr}}$ of Eq. 23 and 24 for $La_2Sn_2O_7$ with data from Paper 3, where it has been assumed that the vibrational modes of $OD_O^{\bullet}$ and D_2O are a factor $\sqrt{2}$ lower than that of $OH_O^{\bullet}$ and H_2O. From the individual contributions, the change in the zero-point energy of H_2O vs. D_2O largely is counteracted by the change in the zero-point energy of the $OH_O^{\bullet}$ vs. $OD_O^{\bullet}$ lattice modes. Similarly, the higher absolute entropy of D_2O than H_2O is counteracted by the entropy change due to reduced

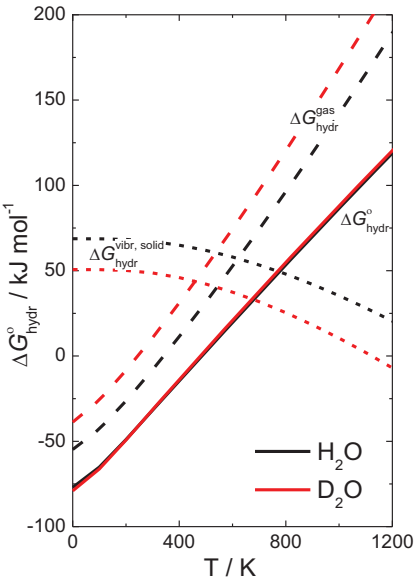

Figure 14: Isotope effect on the Gibbs hydration energy of $La_2Sn_2O_7$ from first principles calculations and thermodynamic modeling.

vibrational frequencies of the $OD_O^\bullet$ defect. As such, the change in ΔG°_{hydr} is small and the resulting ΔH°_{hydr} and ΔS°_{hydr} for H_2O and D_2O amount to -81 kJ mol^{-1} and -82 kJ mol^{-1}, and -167 and -170 J K^{-1}mol^{-1}, respectively. If assuming the electroneutrality in Eq. 17, $p_{H_2O} = p_{D_2O} = 0.025$ atm and an acceptor concentration of for instance 0.10 mole fraction, the concentration ratio of the two defects, $[OH_O^\bullet]/[OD_O^\bullet]$, amounts to 0.93 at 500 K (*i.e.*, when the material is far from saturation by protons/deuterons). Hence, although $[OD_O^\bullet]$ would be marginally higher than $[OH_O^\bullet]$, the difference in the hydration thermodynamics of the two defects are too small to be evaluated from the experimental studies in this work. However, as seen from Eq. 25, the difference in the thermodynamics of hydration by H_2O(g) and D_2O(g) depends on the vibrational frequencies of the $OH_O^\bullet$/ $OD_O^\bullet$ defects, and increasing the frequencies compared to those applied here would increase the isotope effect on ΔH°_{hydr} and ΔS°_{hydr} somewhat.

4.2 Association of hydrogen and cationic acceptor defects

Protons may associate with various ionic acceptor defects, notably cation vacancies and substitutional cationic dopants. Although protons also have been shown to form complexes with anionic acceptors, such as substitutional N defects in the form of $NH_O^\times$, we recently showed that such defects behave more as substitutional NH^{2-} entities [60], and not $N_O^/ + OH_O^\bullet$ complexes [61]. I will therefore limit the following discussion to the more traditional association complexes between $OH_O^\bullet$ and acceptor centers such as cation vacancies (as touched upon in Paper 1, 5-7) and substitutional cationic dopants (notably the $(Li_{Zn}OH_O)^\times$ defect from Paper 7).

Hydrogen and cation vacancies

In Paper 4 we showed, from AC conductivity measurements, that acceptor doped TiO_2 hydrates according to Eq. 18 under both oxidizing and reducing conditions, displaying mix protonic and p-type conduction under oxidizing conditions, and n-type conduction under reducing conditions. From first principles calculations in Paper 5 and 6, however, we showed that the hydration properties of undoped and donor doped TiO_2 will be different from that of the acceptor doped. More specifically, the equilibrium defect chemistry of bulk rutile TiO_2 is largely dominated by cation vacancies, protons and oxygen vacancies, and their mutual association complexes as shown in Figure 15. At lower temperatures the material will hydrate by formation of partly hydrated cation vacancies (so-called Ruetschi type defects [62]) and charge-compensating protons:

$$2H_2O(g) + 2O_O^\times = (v_{Ti}2OH_O)^{//} + 2OH_O^\bullet \qquad (26)$$

and dehydrated cation vacancies at moderately high temperatures:

$$2H_2O(g) + 2O_O^{\times} = v_{Ti}^{4/} + 4OH_O^{\bullet} \quad (27)$$

However, such equilibria may only be reached in thin films or near surface layer, or during growth of the material at low temperatures. Bulk specimens will on the other hand most likely display a non-equilibrium situation in which the concentration of cation vacancies is frozen-in to that formed during for instance sintering. At lower temperatures, the immobile cation vacancies are charge compensated by either protons or oxygen vacancies, as in the acceptor doped case, and hydration is accompanied by formation of the Ruetschi type defects, according to $2\left[(v_{Ti}2OH_O)^{//}\right] = [OH_O^{\bullet}]$. An interesting consequence of vacancy doping of TiO_2 is thus that the total proton concentration is significantly higher than that of for instance Fe doped TiO_2. Further, vacancy doped TiO_2 may also display different hydration thermodynamics than the Fe doped, due to complex formation with the vacancies.

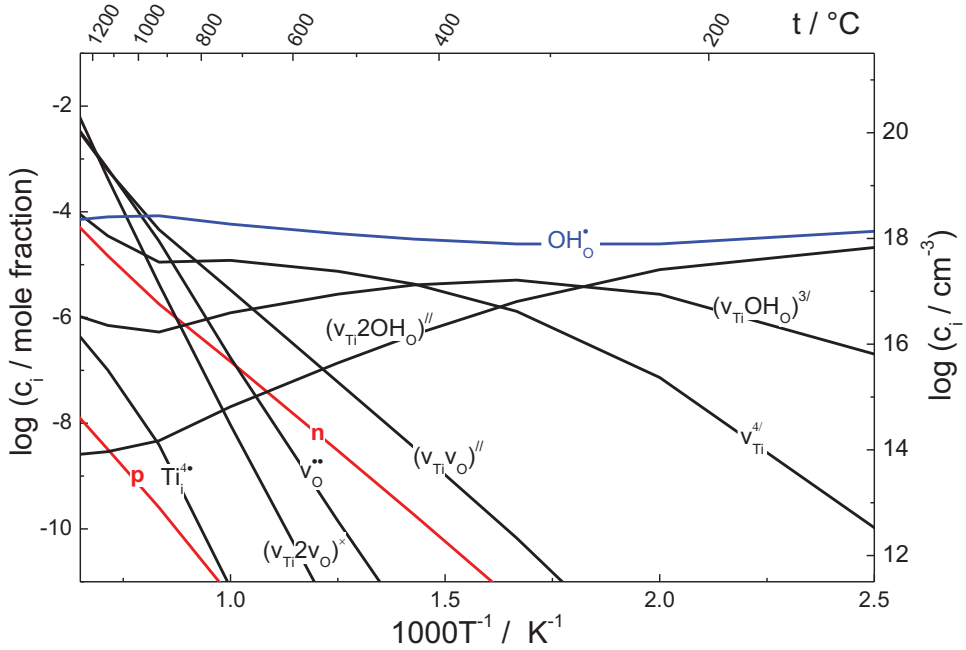

Figure 15: Thermal equilibrium defect concentrations in undoped rutile TiO_2 as a function of inverse temperature with $p_{O_2} = 1$ atm and $p_{H_2O} = 0.025$ atm from Paper 5.

The photocatalytic properties of TiO_2 form the basis of an increasingly popular research field. Although implementation of TiO_2 in technologies such as photocatalytic water purification involves exposure of TiO_2 to humid, oxidizing atmospheres at lower temperatures, cation vacancies and protons have for long been neglected in evaluations of its defect chemistry. However, as shown in this work and speculated by Norby [63], TiO_2 will to a large extent be dominated by such defects. Recently, Nowotny *et al.* [64] attributed a band gap narrowing of 0.1 eV for single crystalline TiO_2 to the formation of the $(v_{Ti}4OH_O)^{\times}$ complex, which is in line

with the shallow acceptor behavior of $v_{Ti}^{4/}$ and $(v_{Ti}nOH_O)^{(4-n)/}$ as shown Paper 5. In Paper 6 we showed that cation vacancies and Ruetschi type defects also are stable at the (1 1 0) surface of rutile TiO_2, especially at lower temperatures under humid conditions, and it is thus foreseeable that these defects play a role in the photocatalytic properties of TiO_2 [65].

Cation vacancies, and their complexes with protons have in the recent years also been proposed to be important in several other binary oxides such as ZnO, SnO_2, In_2O_3 and Ga_2O_3 [66, 67], and one may wonder what determines the dominance of such defects in different oxides. The Schottky formation enthalpies in the structurally different binary oxides, TiO_2, ZnO and Cr_2O_3 according to:

$$\text{null} = v_{Ti}^{4/} + 2v_O^{\bullet\bullet} \tag{28}$$

$$\text{null} = v_{Zn}^{//} + v_O^{\bullet\bullet} \tag{29}$$

$$\text{null} = 2v_{Cr}^{3/} + 3v_O^{\bullet\bullet} \tag{30}$$

amount to 4.6 (1.5), 5.0 (2.5) and 16.9 (3.4) eV per reaction (and per formed defect), respectively, from first principles calculations (see Paper 5 and 7 and footnote 2). Cation vacancies may also form in combination with protons at lower temperatures:

$$2H_2O(g) + 2O_O^{\times} = v_{Ti}^{4/} + 4OH_O^{\bullet} \tag{31}$$

$$H_2O(g) + O_O^{\times} = v_{Zn}^{//} + 2OH_O^{\bullet} \tag{32}$$

$$3H_2O(g) + 3O_O^{\times} = 2v_{Cr}^{3/} + 6OH_O^{\bullet} \tag{33}$$

with calculated reaction enthalpies per reaction (and per defect) of 0.9 (0.2), 4.8 (1.6) and 15.0 (1.9) eV, respectively (for the isolated defects). Hence, protons promote the formation of cation vacancies at lower temperatures compared to the Schottky reactions. Finally, the calculated binding enthalpies of the three complexes $(v_{Ti}OH_O)^{3/}$, $(v_{Zn}OH_O)^{/}$ and $(v_{Cr}OH_O)^{//}$ amount to -0.58, -2.77 and -2.21 eV, respectively. Similarly, the binding enthalpy of the second proton (and third in case of Cr_2O_3) is significantly more exothermic in ZnO and Cr_2O_3, than in TiO_2. However, only in rutile TiO_2 are the vacancies and complexes stable enough to result in an appreciable equilibrium concentration. Figure 16 displays the equilibrium defect structure of ZnO from DFT calculations under the conditions used for rutile TiO_2 in Figure 15. While $v_{Ti}^{4/}$ and $n(v_{Ti}nOH_O)^{(4-n)/}$ dominate TiO_2 completely at lower temperatures (see Figure 15), $v_{Zn}^{//}$ and $(v_{Zn}OH_O)^{/}$ are always in minority with respect to electrons in ZnO. A similar situation may be deduced for Cr_2O_3, and there is seemingly a correlation between the stability of the cation vacancies and their stabilization by protons; the more unstable the

vacancies are, the more negative is the binding enthalpy of their complexes with protons. Further, the stability of neither cation vacancies nor the complexes seemingly correlates with the charge of the cation or the stability of the oxide, as could be expected empirically. This peculiarity may be elaborated upon from the partial DOS for O ions in the bulk oxides, O in $OH_O^{\bullet}$, O coordinated to v_M^q and O in $(v_M OH_O)^q$ for TiO_2 and ZnO (see Figure 17). The most striking difference between the two oxides is the large upward shift in the O states for the O ion coordinated to the cation vacancy in ZnO, which reflects a significant destabilization of the system when breaking the Zn-O bond. In TiO_2, however, the shift is minute, and the destabilization of the system upon formation of v_M^q is thus significantly smaller than for ZnO. These shifts may again be related to the degree of M-O overlap in the bulk oxide; the larger the degree of hybridization of M and O states, the larger is the destabilization of the system upon M removal due to creation of O dangling bonds. Addition of a H to the oxide ion in the form of $(v_M OH_O)^q$ thus stabilizes the system due to termination of these dangling bonds. Hence, the binding enthalpy of the $(v_M OH_O)^q$ complexes stems not from the stability of $OH_O^{\bullet}$ in $(v_M OH_O)^q$ compared to $OH_O^{\bullet}$ (as expected from electrostatic interactions between the charged defects/particles), but from the instability of O around v_M^q. It thus seems that the stability and dominance of cation vacancies in binary oxides to some extent can be correlated

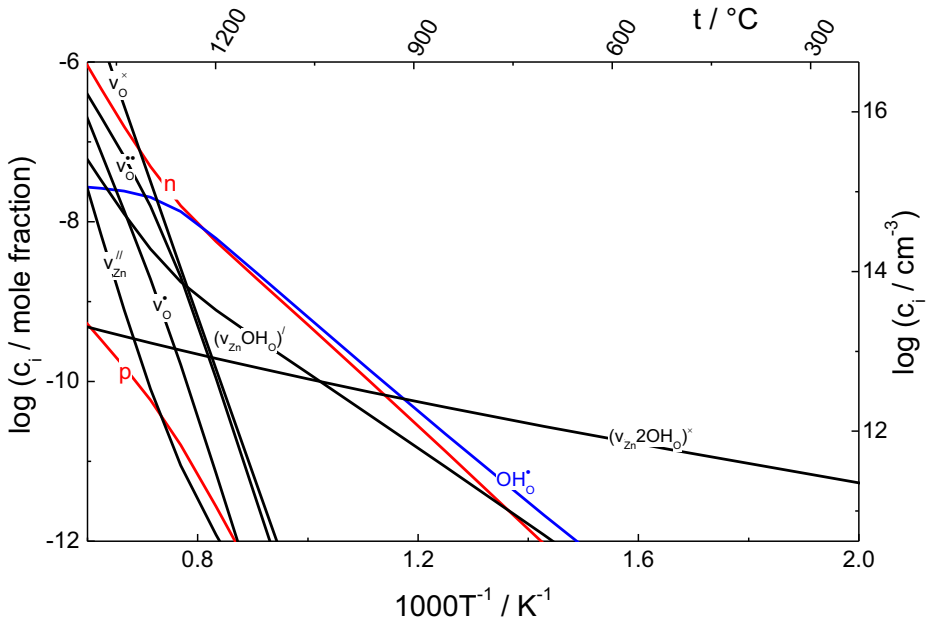

Figure 16: Thermal equilibrium defect concentrations in nominally undoped ZnO as a function of inverse temperature with $p_{O_2} = 1$ atm and $p_{H_2O} = 0.025$ atm as emerging from DFT calculations and thermodynamic modeling.

to the covalency of the oxide; the more covalent the oxide is, the more unstable are cation vacancies and the larger are their binding enthalpies with protons (and also oxygen vacancies).

Finally, in Paper 1, we attributed hydration of $PbZrO_3$ to an electroneutrality in which frozen-in Pb vacancies form the dominating acceptor defects due to the volatile nature of PbO. Owing to the high electronegativity of Pb, and thus the degree of covalency in the Pb-O bond, it is likely that protons associate significantly with $v_{Pb}^{//}$. The determined activation energy of protons in $PbZrO_3$ (0.93 eV) is relatively high compared to that of other cubic perovskites, which possibly can be explained by complex formation with $v_{Pb}^{//}$.

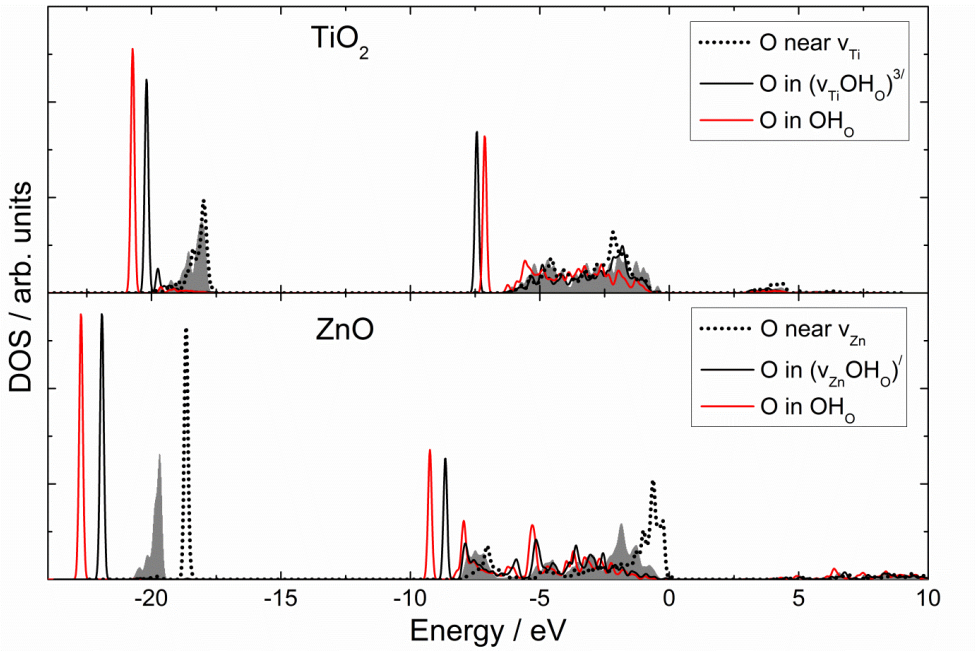

Figure 17: Partial DOS for a bulk O (grey area), O coordinated to v_M (dotted line), O in $(v_M OH_O)^q$ (black solid) and O ion the $OH_O^{\bullet}$ defect (red) in TiO_2 and ZnO from DFT-HSE calculations. The energies are set with reference to the valence band maximum.

Hydrogen and Li in ZnO

In an effort to elaborate on the possibility of p-type doping of ZnO, we reported the effect of protons on the defect chemical and electrical properties of Li doped ZnO in Paper 7. Li dissolves both as a substitutional acceptor and an interstitial donor in ZnO, and reduces the native n-type conductivity of as-grown ZnO due to compensation by ionic defects:

$$2[v_O^{\bullet\bullet}] + [OH_O^{\bullet}] + [Li_i^{\bullet}] = [Li_{Zn}^{/}] \qquad (34)$$

Under humid conditions at lower temperatures, we also indicated that the majority of Li'_{Zn} is bound in the complex $(Li_{Zn}OH_O)^{\times}$, with a DFT determined binding enthalpy of -0.9 eV. Splitting of this complex yields an activation energy of the proton conductivity of ~1.6 eV, which is significantly higher than in the majority of other acceptor doped proton conductors. While for instance perovskite (AXO_3), monazite ($REXO_4$) and pyrochlore ($RE_2X_2O_7$) structured proton conductors usually are doped with chemically similar elements, resulting in only modest binding enthalpies of protons with the acceptor [10, 33, 68], the pronounced binding enthalpy of $(Li_{Zn}OH_O)^{\times}$ may be attributed to the more ionic nature of Li than Zn. As for the $(v_{Zn}OH_O)^{/}$ complex, the binding enthalpy of $(Li_{Zn}OH_O)^{\times}$ is thus due to the instability of O ions coordinated to Li'_{Zn} compared to bulk O, and not simply electrostatic interactions between the two charged defects.

5. Conclusions and outlook

The present thesis has taken on fundamental studies of the behavior of hydrogen in a wide range of oxides with different functional properties. The work is focused on the binary oxides TiO_2 and ZnO and a range of perovskite (*e.g.* $PbZrO_3$), monazite (*e.g.* $LaAsO_4$) and pyrochlore (*e.g.* $La_2Sn_2O_7$) structured oxides, and employs both experimental electrochemical techniques and computational first principles investigations.

AC conductivity measurements have shown that acceptor doped and Pb deficient $PbZrO_3$ is a mixed p-type electronic and protonic conductor to moderately high temperatures in wet, oxidizing atmospheres. The mobility enthalpy of protons was determined to 0.93 eV for nominally Y doped $PbZrO_3$, which is in the upper limit of similar perovskites, and may possibly be a result of association with Pb vacancies. The results further show that the hydration enthalpy of perovskite oxides correlates with the absolute value of the electronegativity difference of the cations, but also with the Goldschmidt tolerance factor, indicating that changes in both bonding nature and symmetry through the series affect the hydration enthalpies

Acceptor doped $LaAsO_4$ was found to be a modest proton conductor, with partial proton conductivities lower than those reported for $LaPO_4$. Although substituting P with the larger As lowers the activation energy of the proton mobility slightly, a lower pre-exponential mobility yields an overall lower proton conductivity. Finally, the hydration thermodynamics are found to be comparable through the $LaXO_4$ (X = P, As and V) series, despite the difference in the chemical nature of P/As and V.

TG measurements and DFT calculations show that the hydration enthalpy of $RE_2X_2O_7$ (RE = La-Lu, X = Ti, Sn, Zr and Ce) pyrochlore structured oxides increases notably (less exothermic) with decreasing radii of the RE ions, while it is less affected by the X ion, similar to as in the $LaXO_4$ (X = P, As and V) series. We attribute this to effects from destabilization of the oxide and changes in bonding nature which are additive when changing the RE element from La to Lu, but to some extent counteracting when changing the X site element.

As shown in the thesis, the behavior of hydrogen in oxides is not limited to the protonic defect. Our DFT calculations suggest that hydride ions substituting oxide ions may be more

important in oxides than previously assumed. We indicate that such defects may dominate wide band gap semiconductors under the most reducing conditions at higher temperatures, where they are charge-compensated by electrons. Based on these results, we suggest that such defects may be the cause of reports of transport of apparent negative or neutral hydrogen species in solid state ionics research the last decade.

Protons may form complexes with a variety of negatively charged defects, notably cation vacancies or substitutional dopants. DFT calculations in this work suggest that partly protonated cation vacancies, or Ruetschi defects, will dominate undoped and donor doped bulk, and also the surfaces of rutile TiO_2 in wet atmospheres at lower temperatures. Schottky disorder dominates at higher temperatures, and quenching of rutile TiO_2 may thus result in effective vacancy doping. In other binary oxides touched upon in this work, notably ZnO and Cr_2O_3, the Schottky formation energies are significantly higher, yielding only minute cation vacancies concentrations. However, the stabilization of cation vacancies by protons (*i.e.,* the binding enthalpy) becomes more exothermic with increasing Schottky formation energies, and the cation vacancies in ZnO and Cr_2O_3 will to a larger extent be present as Ruetschi defects than in rutile TiO_2. We suggest that this may be related to the covalency of the oxides; increasing covalency results in increasing destabilization of the surrounding oxide ions upon cation vacancy formation. The more unstable the oxide ions in the cation vacant oxide are, the more they are stabilized by protonic defects.

DFT calculations and electrical measurements on ZnO indicate that the difficulties in effective p-type doping of ZnO with Li are due to charge-compensation of the Li acceptor, $Li_{Zn}^{/}$, by the donor defects $v_O^{\bullet\bullet}$, $OH_O^{\bullet}$ and $Li_i^{\bullet}$. Further, at lower temperatures $Li_{Zn}^{/}$ is also passivated in the form of the effectively neutral complexes $(Li_{Zn}OH_O)^{\times}$ and $(Li_{Zn}Li_i)^{\times}$. Hence, although Li doping lowers the Fermi level of ZnO, the material remains n-type under internal equilibrium. We however suggest that one might lower the Fermi level even further under non-equilibrium conditions by quenching of ZnO from higher temperatures followed by post annealing. Another interesting approach would be doping of ZnO by the larger alkali metals Na or K as their larger ionic radii would increase the concentration ratio of the substitutional acceptor and the interstitial donor defect.

The thesis emphasizes the importance of computational first principles techniques in materials research. While such techniques earlier have suffered from the shortcomings of traditional exchange-correlation functionals, the rapid increase in computational resources has allowed routine application of more sophisticated techniques such as hybrid functionals. While hybrid functionals, which by intermixing a fraction of exact Hartree-Fock exchange, overcome for instance the underestimated band gaps of LDA/GGA based functionals, such functionals are still limited to small supercells of up to 100 atoms in practical calculations. Improved computational resources will in the future pave the way for utilization of such functionals for

larger systems, thus enabling for instance more accurate determination of defect properties. Similarly, increased computing power may allow application of hybrid functionals in phonon calculations and large scale molecular dynamics simulations, thus allowing accurate predictions of for instance transport properties of protons at finite temperatures. In conclusion, I believe the interest in such techniques in the recent years only is the early stage, and I would expect that first principles calculations in the future will be routinely adopted by both experimentalist and theoreticians alike.

References

1. M. S. Islam, *Journal of Materials Chemistry*, 2000, **10**, 1027-1038.
2. L. Minervini, R. W. Grimes and K. E. Sickafus, *Journal of the American Ceramic Society*, 2000, **83**, 1873-1878.
3. C. R. Stanek, L. Minervini and R. W. Grimes, *Journal of the American Ceramic Society*, 2002, **85**, 2792-2798.
4. E. Kendrick, M. S. Islam and P. R. Slater, *Journal of Materials Chemistry*, 2007, **17**, 3104-3111.
5. M. S. Islam and P. R. Slater, *MRS Bulletin*, 2009, **34**, 935-941.
6. P. Hohenberg and W. Kohn, *Physical Review*, 1964, **136**, B864-B871.
7. W. Kohn and L. J. Sham, *Physical Review*, 1965, **140**, A1133-A1138.
8. J. Hafner, C. Wolverton and G. Ceder, *MRS Bulletin*, 2006, **31**, 659-668.
9. J. Hafner, *Journal of Computational Chemistry*, 2008, **29**, 2044-2078.
10. M. Huse, Ph.D. Thesis, University of Oslo, 2011.
11. D. G. Thomas and J. J. Lander, *The Journal of Chemical Physics*, 1956, **25**, 1136-1142.
12. C. G. Van de Walle and J. Neugebauer, *Nature*, 2003, **423**, 626-628.
13. S. Steinsvik, Y. Larring and T. Norby, *Solid State Ionics*, 2001, **143**, 103-116.
14. F. W. Poulsen, *Solid State Ionics*, 2001, **145**, 387-397.
15. T. Norby, M. Widerøe, R. Glöckner and Y. Larring, *Dalton Transactions*, 2004, 3012-3018.
16. M. Widerøe, R. Waser and T. Norby, *Solid State Ionics*, 2006, **177**, 1469-1476.
17. A. Janotti and C. G. Van de Walle, *Nature Materials*, 2007, **6**, 44-47.
18. J. P. Perdew and A. Zunger, *Physical Review B*, 1981, **23**, 5048-5079.
19. J. P. Perdew and Y. Wang, *Physical Review B*, 1992, **45**, 13244-13249.
20. J. P. Perdew, K. Burke and M. Ernzerhof, *Physical Review Letters*, 1996, **77**, 3865.
21. J. Heyd, G. E. Scuseria and M. Ernzerhof, *The Journal of Chemical Physics*, 2003, **118**, 8207-8215.
22. J. Heyd, G. E. Scuseria and M. Ernzerhof, *The Journal of Chemical Physics*, 2006, **124**, 219906-219901.
23. F. Oba, A. Togo, I. Tanaka, J. Paier and G. Kresse, *Physical Review B*, 2008, **77**, 245202.
24. A. Janotti, J. B. Varley, P. Rinke, N. Umezawa, G. Kresse and C. G. Van de Walle, *Physical Review B*, 2010, **81**, 085212.
25. G. Kresse and J. Hafner, *Physical Review B*, 1993, **47**, 558-561.
26. G. Kresse and J. Hafner, *Physical Review B*, 1994, **49**, 14251-14269.
27. G. Kresse and J. Furthmüller, *Physical Review B*, 1996, **54**, 11169.
28. G. Kresse and J. Furthmüller, *Computational Materials Science*, 1996, **6**, 15-50.
29. K. Schwarz, P. Blaha and G. K. H. Madsen, *Computer Physics Communications*, 2002, **147**, 71-76.
30. P. E. Blöchl, *Physical Review B*, 1994, **50**, 17953.
31. F. Oba, M. Choi, A. Togo and I. Tanaka, *Science and Technology of Advanced Materials*, 2011, **12**, 034302.
32. T. Mattila and A. Zunger, *Physical Review B*, 1998, **58**, 1367.
33. M. E. Björketun, P. G. Sundell and G. Wahnström, *Faraday Discussions*, 2007, **134**, 247-265.
34. J. Maier, *Physical Chemistry of Ionic Materials: Ions and Electrons in Solids*, John Wiley & Sonds LTD, England, 2004.
35. A. Janotti and C. G. Van de Walle, *Applied Physics Letters*, 2005, **87**, 122102-122103.
36. S. Lany and A. Zunger, *Physical Review B*, 2010, **81**, 113201.
37. J.-R. Martinez, C. E. Mohn, S. Stølen and R. Søndenå, *Physical Chemistry Chemical Physics*, 2006, **8**, 2036-2039.
38. J. Paier, R. Hirschl, M. Marsman and G. Kresse, *The Journal of Chemical Physics*, 2005, **122**, 234102-234113.
39. G. Kresse and J. Hafner, *Surface Science*, 2000, **459**, 287-302.
40. A. Bilić and J. D. Gale, *Physical Review B*, 2009, **79**, 174107.
41. K. Tsuda and M. Tanaka, *Acta Crystallographica Section A*, 1995, **51**, 7-19.

42. N. Bork, N. Bonanos, J. Rossmeisl and T. Vegge, *Physical Chemistry Chemical Physics*, 2011, **13**, 15256-15263.
43. T. S. Bjørheim, S. Stølen and T. Norby, *Physical Chemistry Chemical Physics*, 2010, **12**, 6817-6825.
44. C. A. Bridges, G. R. Darling, M. A. Hayward and M. J. Rosseinsky, *Journal of the American Chemical Society*, 2005, **127**, 5996-6011.
45. C. A. Bridges, F. Fernandez-Alonso, J. P. Goff and M. J. Rosseinsky, *Advanced Materials*, 2006, **18**, 3304-3308.
46. Y. Kobayashi, O. J. Hernandez, T. Sakaguchi, T. Yajima, T. Roisnel, Y. Tsujimoto, M. Morita, Y. Noda, Y. Mogami, A. Kitada, M. Ohkura, S. Hosokawa, Z. Li, K. Hayashi, Y. Kusano, J. E. Kim, N. Tsuji, A. Fujiwara, Y. Matsushita, K. Yoshimura, K. Takegoshi, M. Inoue, M. Takano and H. Kageyama, *Nature Materials*, 2012, **advance online publication**.
47. E. V. Lavrov, F. Herklotz and J. Weber, *Physical Review B*, 2009, **79**, 165210.
48. S. G. Koch, E. V. Lavrov and J. Weber, *Physical Review Letters*, 2012, **108**, 165501.
49. C. Kongshaug, Ph.D. Thesis, University of Oslo, 2010.
50. A. Janotti and C. G. Van de Walle, *Nature Materials*, 2007, **6**, 44-47.
51. Y. Larring and T. Norby, *Solid State Ionics*, 1995, **77**, 147-151.
52. T. Norby and Y. Larring, *Current Opinion in Solid State and Materials Science*, 1997, **2**, 593-599.
53. K. D. Kreuer, *Solid State Ionics*, 1999, **125**, 285-302.
54. K. D. Kreuer, S. Adams, W. Münch, A. Fuchs, U. Klock and J. Maier, *Solid State Ionics*, 2001, **145**, 295-306.
55. T. Tauer, R. O'Hayre and J. W. Medlin, *Solid State Ionics*, 2011, **204–205**, 27-34.
56. K. D. Kreuer, *Annual Review of Materials Research*, 2003, **33**, 333-359.
57. R. Haugsrud, Y. Larring and T. Norby, *Solid State Ionics*, 2005, **176**, 2957-2961.
58. L. R. Morss, *Journal of the Less Common Metals*, 1983, **93**, 301-321.
59. J. Goudiakas, R. G. Haire and J. Fuger, *The Journal of Chemical Thermodynamics*, 1990, **22**, 577-587.
60. X. Li, B. Keyes, S. Asher, S. B. Zhang, S.-H. Wei, T. J. Coutts, S. Limpijumnong and C. G. Van de Walle, *Applied Physics Letters*, 2005, **86**, 122107-122103.
61. J. M. Polfus, T. S. Bjørheim, T. Norby and R. Haugsrud, *Physical Chemistry Chemical Physics*, 2012, **14**, 11808-11815.
62. P. Ruetschi, *Journal of The Electrochemical Society*, 1984, **131**, 2737-2744.
63. T. Norby, *MRS Bulletin*, 2009, **34**, 923-928
64. J. Nowotny, *The Journal of Physical Chemistry C*, 2011, **115**, 18316-18326.
65. J. Nowotny, T. Norby and T. Bak, *The Journal of Physical Chemistry C*, 2010, **114**, 18215-18221.
66. K. M. Johansen, H. Haug, E. Lund, E. V. Monakhov and B. G. Svensson, *Applied Physics Letters*, 2010, **97**, 211907-211903.
67. J. B. Varley, H. Peelaers, A. Janotti and C. G. Van de Walle, *Journal of Physics: Condensed Matter*, 2011, **23**, 334212.
68. M. E. Björketun, C. S. Knee, B. J. Nyman and G. Wahnström, *Solid State Ionics*, 2008, **178**, 1642-1647.